Journal of Mathematical Chemistry Vol. 42, No. 1, July 2007 (© 2007)
DOI: 10.1007/s10910-007-9227-9

Decisive role of mathematical methods in early cancer diagnostics: optimized Padé-based magnetic resonance spectroscopy

Dževad Belkić[1,*] and Karen Belkić[1,2]

[1] *Department of Oncology and Pathology, Karolinska Institute, P.O. Box 260, Stockholm, SE-171776, Sweden*
E-mail: Dzevad.Belkic@ki.se

[2] *Institute for Prevention Research, The University of Southern California School of Medicine, Los Angeles, CA, USA*

Received 14 December 2006; revised 12 January 2007

Key to cancer treatment and overall tumor control is early diagnostics. Remarkably, Magnetic Resonance (MR) physics with the underlying mathematics for the reconstruction problems plays a pivotal role not only for early tumor diagnosis, but also for target definition, dose planning systems and therapy. The overall goal of this review is to highlight certain novel mathematical methods for improvement of cancer diagnostics on a quantitative molecular basis by retrieving key information which remains undetected with standard data analysis. We intend to contribute to a large effort aimed at establishing Magnetic Resonance Spectroscopy (MRS) and Magnetic Resonance Spectroscopic Imaging (MRSI) as two standard diagnostic tools for clinical oncology, with their complementary roles relative to anatomical information provided by Magnetic Resonance Imaging (MRI). Crucially, such efforts are within the realm of mathematical descriptions of data measured by the MR methods and the related physical, chemical and biomedical interpretations. This can be achieved with fidelity by applying the fast Padé transform (FPT) to MRI, MRS and MRSI. Thus far, we have completed the "proof of principle" investigations demonstrating that the FPT is a powerful, stable parametric processor with robust error analysis, which provides unequivocal quantification of *in vivo* time signals encoded via MRS. These are the most stringent criteria imposed upon MRS and MRSI by clinical oncology. The established overall reliability of the FPT firmly justifies the present suggestion for undertaking further extensive applications of the FPT to a variety of phantom and clinical time signals at vastly different magnetic field strengths, with a broad range of signal-to-noise ratio (SNR). This would enable Padé-based MRI, MRS and MRSI to soon join the standard diagnostic armamentarium for clinical practice, especially in oncology. Of particular importance is to extend the current applications of the FPT to *in vivo* MRS signals encoded from patients with e.g. breast, prostate and ovarian cancers, so as to compare the obtained results with findings from non-malignant tissue, that have presented differential diagnostic dilemmas,

* Corresponding author.

notably benign tumors, infectious or inflammatory lesions. The fact that the FPT is capable of extracting unambiguous quantitative information from tissue via mathematical parametric analysis can be exploited to develop normative data bases for metabolite concentrations versus the corresponding findings seen in malignancy. This would provide the needed standards to aid in cancer diagnostics, identifying malignant versus benign disease with specific patterns of departures from normal metabolite concentrations. Overall, this succinct review focuses on the benefits from a judicious intertwining of spectral analysis from mathematics with quantum-mechanical signal processing from physics as well chemistry, especially when these basic sciences are used synergistically to enhance the diagnostic power of MRI, MRS and MRSI in clinical oncology.

KEY WORDS: Padé approximant, fast Padé transform, spectral analysis, signal processing, quantification, early cancer diagnostics

1. Introduction

1.1. Main features of the fast Padé transform, FPT

The FPT is an eigenproblem solver from the family of the well-established Padé approximant (PA), given by a polynomial quotient P/Q, which is undoubtedly the most often used mathematical model for rational response functions in vastly different scientific, technological and industrial research fields, ranging from speech processing, circuit theory, heart-rate variability, acoustics, statistics, system theory, mobile phone communications, pharmacokinetics, bio-medical engineering, milling machine industry, etc [1]. Numerical analysis in every computer mainframe and mathematical software packages are literally inundated by the Stieltjes continued fractions, as one of the most stable algorithms of the PA, even for the most elementary Taylor or Maclaurin series expansions of trigonometric, exponential, or special functions, etc [1]. The fact that the PA has already made gigantic strides across interdisciplinary research comes as no surprise by reference to quantum physics whose finite-rank response function (Heisenberg's S-matrix element, Green's function, Schwinger's variational principle, Fredholm's determinant) [1,2] to any external perturbation is given by precisely the same polynomial quotient as in the Padé approximant.

The PA has been reinvented under some other names in various disciplines, e.g. in signal processing where it is known as the Auto-Regressive Moving Average (ARMA). Another clearly most important mathematical tool for the analysis of linear discrete systems, known as the causal z-transform (ZT) [1], also reduces to the usual PA. The ZT is a Maclaurin series development in powers of a complex variable z, i.e. $\sum_n c_n z^{-n}$, with the expansion coefficients $\{c_n\}$ as a given sequence of numbers. In signal processing, these expansion coefficients $\{c_n\}$ are the known time signal points, or discretized auto-correlation functions, and z is the harmonic variable defined as a frequency-dependent complex damped exponential. In such a case, the ZT represents a spectrum in the frequency domain.

There exists also the corresponding anti-causal z-transform which reduces to the PA, as well. When such explicit reductions in the causal and anti-causal ZT are carried out, the causal and anti-causal Padé z-transform (PZT) are obtained, respectively. The FPT is a theoretical and algorithmic unification of the causal and anti-causal PZT into a single framework [1]. Moreover, a single formula exists in the form of the so-called contracted continued fractions (CCF) whose odd and even parts represent the causal and anti-causal PZT, respectively [1].

Importantly, the analytical expression for the general expansion coefficient a_n in the CCF has recently been derived [1] for the given Maclaurin series $\sum_n c_n z^{-n}$ with any model-free input data $\{c_n\}$. Since, just like the ZT itself, an arbitrary finite-order CCF also reduces either to the causal or the anti-causal PZT, the availability of the closed expression for a_n automatically provides the analytical expressions for the polynomial quotients P/Q in the FPT. Such analytical expressions for the expansion coefficients of the numerator (P) and denominator (Q) polynomial serve as the benchmark data or the gold standard for verification of all the alternative numerical algorithms.

Furthermore, certain limiting values of the expansion coefficients of the CCF yield the highly accurate zeros of Q, as in the well-known Rutishauser quotient-difference (QD) algorithm, and these are simultaneously the poles of the spectrum P/Q, since this latter quotient is a meromorphic function (a function whose sole singularities are poles). The significance of such a simple procedure is in finding all the poles in the investigated spectrum without resorting to any classical root-searching routines, e.g. the characteristic polynomial equation ($Q = 0$) or the corresponding equivalent eigenvalue problem (Hessenberg's matrix eigenvalue problem). Moreover, once all the poles of P/Q have been found in this straightforward and easy way, the associated amplitudes can also be readily obtained in the FPT from yet another analytical expression as the Cauchy residue of the quotient P/Q. With this accomplishment, the FPT becomes a unique signal processor which carries out the entire spectral analysis, i.e. solves the quantification problem by using exclusively the analytical, closed formulae. This is a veritable breakthrough, especially given that this latter problem is a notoriously ill-conditioned inverse problem when solved by any of the alternative numerical algorithms [1].

1.2. Survey of the field from a clinical viewpoint

1.2.1. Magnetic Resonance-based cancer diagnostics: a brief overview of achievements to date with standard data analytical techniques

First we will present MR-based methods that are becoming the modality of choice for a rapidly expanding range of applications in oncology. For example, MRI [3] being non-invasive, highly sensitive and free from ionizing radiation, is indispensable for timely detection of many cancers. However, MRI often

has poor specificity. Molecular imaging through MRS can enhance specificity by detecting metabolic features characteristic of malignancy.[1] Also, *molecular changes often precede morphologic alterations, so that sensitivity can be further improved by MRS*. This kind of molecular imaging is becoming widely appreciated as an extraordinary opportunity for early disease detection, by identifying key changes for the emergence and progression of cancer on the molecular level. The combination of anatomic localization and insight into metabolic characteristics from spectral information is often decisive for accurate and timely identification of malignancy. This can be invaluable, especially in difficult cases, e.g. differentiating recurrent tumor from radiation necrosis or post-operative changes. These advantages have become particularly clear in neuro-oncology, where MRI and MRS now are a key modality for brain tumor diagnostics [4–7]. Clinical MR-based tools are a cornerstone of modern neuro-diagnostics in general, with MRS becoming increasingly appreciated [8,9]. These tools have also made an impact on prostate cancer providing diagnostic clarity unmatched by literally any other non-invasive method [7,10–12]. Moreover, MRI and MRS have improved diagnostic accuracy for e.g. breast cancer [13], non-Hodgkin's lymphoma[2] [14,15], as well as head and neck cancers [16,17].

Notwithstanding these achievements, there are still important shortcomings of current applications of *in vivo* MRS to clinical oncology that have hampered wider implementation of this method in cancer diagnostics. Very few of the metabolite concentrations or their ratios estimated in the standard way unequivocally distinguish tumors from normal tissue, nor are these specific for cancer. Infection, infarction and demyelinating disorders, e.g. frequently show spectral changes identical to those of brain tumors. Histopathological characterization and brain tumor grading have been greatly aided by MRS. Nevertheless, there are numerous contradictory findings in the literature. Particularly troublesome is the limited possibility of MRS to detect very small tumors. For breast cancer diagnostics using MRS, this is especially problematic, due to the need for lipid suppression. A current strategy has been to increase echo time (TE), to decrease overlap with lipid signal, but this is achieved by a diminution in signal intensity. Also, metabolites with short T_2 relaxation times will have decayed at longer TE; e.g. myoinositol whose estimated concentrations best distinguished breast cancer from a fibroadenoma in our analysis [18,19] of *in vitro* MRS data [20]. Poor SNR is a major cause of false negative findings using MRS to detect malignant breast lesions [13]. Breast cancer detection through MRS has mainly relied upon the presence or absence of a composite (total) choline peak. This compromises

[1]Unless otherwise denoted, MRS will be primarily referring to proton MRS, which is also denoted as ^{1}H MRS. However, this does not mean that the FPT is restricted to ^{1}H MRS. Quite the contrary, the FPT has no restriction whatsoever as to the type of resonating nuclei.

[2]As to the diagnosis of non-Hodgkin's lymphoma via MRS, mainly ^{31}P MRS has thus far been used.

diagnostic accuracy, since choline may be observed in benign breast lesions and in normal breast during lactation. Furthermore, choline is often undetected in small tumors that are then misclassified as benign [13].

Metabolite ratios are also problematic, being dependent upon TE [21], and affected by confounding factors including cancer treatment itself. Consequently, malignancy-defining ratio cut-points vary widely from author to author, as reviewed recently in Ref. [7]. Even for prostate cancer diagnostics, where choline-to-citrate ratios are of major help, dilemmas often arise. For example, in stromal tissue or metabolic atrophy, citrate levels are low without cancer being present, or with prostatic hypertrophy, citrate can still be high despite coexistent malignancy [7]. For detecting tumors in deep-seated, moving organs, applications of MRS are hampered by poor SNR [14]. A case in point is the ovary where early cancer detection is still beyond current reach. Because of the small size and motion of this organ, *in vivo* MRS is mired by problems of resolution and SNR, and yet, there is a rich store of MR-observable compounds that distinguish benign from cancerous adnexal masses when *in vitro* MRS with its attendant high resolution is applied [22–25]. It has been suggested that insofar as the current problems hindering encoding of high quality time signals and their subsequent spectral analysis are overcome, *in vivo* ^{1}H MRS could become the method of choice for evaluating ovarian lesions [25].

1.2.2. Optimization of MRS for early cancer detection needs more advanced signal processing methods

As described in the next sub-section, many problems with current applications of MRS within clinical oncology are directly related to a heavy reliance upon the conventional signal processing method, i.e. the fast Fourier transform (FFT). Optimization of MRS for timely cancer detection requires more advanced signal processing than FFT. One may wonder: how could mathematics play such a critical role in medical diagnostics? This is the case because data encoded directly from patients by means of existing imaging techniques, e.g. CT (computerized tomography) or PET (positron emission tomography), as well as MRI [26] and MRS [1,27] are not at all amenable to direct interpretation which, therefore, need mathematics via signal processing.

2. Standard and novel signal processing methods

2.1. Standard estimation: limitations of the fast Fourier transform

The FFT has been widely used for data processing in clinical research because of its steady convergence with increasing signal length N at a selected bandwidth (or equivalently, with increasing acquisition time T) , such that reasonable looking MR shape spectra can usually be obtained for not so severely

truncated time signals.[3] This steady convergence means that there are no major troublesome surprises for varying signal lengths. In sharp contrast, nearly all parametric estimators show marked instability as a function of the signal length. This is manifested in dramatic oscillations (e.g. spikes and other artificial spectral structures) that appear prior to convergence, if at all, as emphasized in Refs. [1,27]. Needless to say, such spurious findings are anathema to the clinical demands for reliable spectral information aimed at aiding diagnostics.

Although computationally stable, the FFT is nevertheless a low-resolution shape estimator. Within the FFT, a complex-valued Fourier spectrum is defined by using only *a single polynomial*:

$$F \equiv F_k = \frac{1}{N} \sum_{n=0}^{N-1} c_n e^{2i\pi nk/N} \quad (0 \leqslant k \leqslant N-1), \tag{1}$$

where the expansion coefficients $\{c_n\}$ are the time signal points. Resolution $2\pi/T$ in the FFT is pre-determined exclusively by the total acquisition time $T = N\tau$, where τ is the sampling time. The FFT spectrum is defined *only* on the Fourier grid points $2\pi k/T (k = 0, 1, \ldots, N-1)$. The standard strategy applied in attempts to improve resolution has been to increase T and thereby decrease the distance $2\pi/T$ between any two adjacent equidistant grid-points. This does not solve the problem at all, because MRS signals become heavily corrupted with background noise at longer T. Since these time signals decay exponentially as a free induction decay (FID) curve, larger signal intensities are observed early in the encoding. It is, therefore, advantageous to rapidly encode FIDs, avoiding long T in which case mainly noise is measured. Thus, there are two mutually exclusive requirements within the FFT whose attempts to improve resolution lead to worsened SNR. The FFT is a linear transform and, therefore, imports noise as intact from the time to the frequency domain, further contributing to poor SNR [1]. Moreover, the FFT has no extrapolation property based upon the encoded FID.

The FFT is limited to non-parametric estimation, thus providing only the total shape or envelope of spectral structures, *but not their quantifications*. Peak parameters are subsequently extracted in post-processing by various fitting devices whose most severe drawback is non-uniqueness. This means that e.g. 2, 3 or more resonances can yield the same fit to a given structure, with no way to tell which of the fits is correct. These problems are most pronounced for overlapping resonances, which are often clinically important [28]. Many contradictory findings are related to whether or not a given metabolite was included in the

[3]In practice, all experimental time signals are truncated, since infinitely long signals required by the exact Fourier analysis cannot be measured. This is not critical for relatively long signals, but considerable spectral deformation (Gibbs ringing) can arise for severe truncations, i.e. for shorter total acquisition times.

original expansion basis set for fitting [29,30]. Besides the fact that fitting is non-unique, much information contained in the signal is not obtained in an adequate way, such that estimates for position, width, height and phase of resonances can be biased, despite a deceptive decline in the assessed Kramer-Rao error bounds. This is due to the non-orthogonality of basis set elements used in fittings with a serious deficiency that any change in one or more adjustable parameters could largely be compensated by independent alterations in the remaining parameters, as pointed out in Ref. [27]. Moreover, fitting algorithms require some initial values for the sought spectral parameters (complex frequencies and amplitudes). Such starting values are unknown and they are guessed. Different guesses lead to different sets of estimates for the spectral parameters. This indicates that different local minima are found (as opposed to the correct, global minimum), thus pointing to the non-reliability of all standard least square fitting routines. Metabolite concentrations can only be accurately computed if the spectral parameters are obtained in a reliable way with an intrinsic and robust error analysis, as in the FPT. The vital need for this quantitative information has been repeatedly underscored with respect to MRS for cancer diagnostics [7–9,13,25,28].

2.2. *Novel estimation: advantages of fast Padé transform with specific relevance for MRS applications to cancer diagnostics*

In our recent publications [1,27,31–44], it has been conclusively demonstrated that the FPT can overcome simultaneously all the above-described limitations of the FFT, that are of critical relevance for MRS applications to cancer diagnostics. The FPT is a non-linear *polynomial quotient* P_L/Q_K of the exact finite-rank spectrum (the Green function) given by the Maclaurin series with the encoded raw time signal $\{c_n\}$ as the expansion coefficients. Non-linearity of the FPT yields noise suppression. The FPT shares the most favorable property of the FFT, i.e. the FPT is a stable signal processor when the signal length is systematically augmented, producing no spikes or other spectral deformations [1, 41]. In contrast to the FFT, the FPT is a powerful interpolator and extrapolator. Due to extrapolation, which is present in the implicit polynomial inversion via Q_K^{-1} in P_L/Q_K, inference is gained from a non-measurable infinite number of time signal points by using only the available finite set $\{c_n\}$ ($0 \leqslant n \leqslant N-1, N < \infty$). The FPT can use the fixed Fourier mesh $2\pi k/T (k = 0, \ldots, N-1)$, but it is not limited to this grid, as opposed to the FFT. In other words, the FPT can be computed at any frequency ω. Resolution in the FPT is not pre-determined by T, in contradistinction with the FFT. Moreover, the FPT has a better resolving power, relative to the FFT. Rapid convergence, improved SNR, enhanced resolution and robust error analysis result in markedly improved information content extracted by the FPT from *in vivo* MRS signals. These favorable features of the FPT have explicitly been demonstrated in Refs. [1,27,41] via detailed

comparisons of the FPT with the FFT using clinical *in vivo* MRS FIDs. Similarly, we have checked that the FPT outperforms a number of parametric estimators, such as the Hankel-Lanczos Singular Value Decomposition (HLSVD) [45], Variable Projection Method (VARPRO) [46], Advanced Method for Accurate Robust and Efficient Spectral Fitting (AMARES) [47], Linear Combination of Model *in vitro* Spectra (LCModel) [48], etc.

Recently in Refs. [1,34–39] elaboration and validation is provided for a number of powerful computational algorithms by which the FPT yields quantitative spectral parameters. This is done without fitting and the solution is unique. The FPT retrieves with fidelity overlapping or hidden resonances [1] that are often of critical clinical relevance, as mentioned. Most recently, we have reported explicitly on reconstruction of spectral parameters from FIDs of the type customarily encoded clinically from healthy human brain by means of MRS [42–44]. With this accomplishment, it is thereby demonstrated that the FPT identifies and unequivocally quantifies all physical resonances, including overlapping peaks that are customarily left undetected by the FFT [1,42–44,49].

In this review, we shall expound the main ideas, goals and methods derived from the basic interdisciplinary research on MRS and MRSI that sprang from a judicious intertwining of quantum physics, mathematics, chemistry and medicine. The roadmap for a comprehensive strategy emanating from this review has been set in the two recent books on the subject covering the mathematical/physical [1] and clinical [7] aspects of the problem. In Ref. [1] thorough comparative analyses were performed of virtually all the significant signal processors available to MRS, such as the Lanczos Algorithm (LA), HLSVD, linear predictor (LP), Padé-Laplace transform, Prony method, causal/anticausal z-transform, beam-space diagonalization methods, Filter Diagonalization (FD), Decimated Signal Diagonalization (DSD), Decimated Linear Predictor (DLP), decimated Padé approximant (DPA), power and modified moment problem, quotient-difference (QD) (Rutishauser), product-difference (PD) (Gordon), continued fractions (CF) (Stieltjes), etc. As a net outcome of such detailed testing, the FPT emerged as the method of choice for MR physics in medicine and biology. One of the useful side-products of such an undertaking is the acquired expertise for the usage of many estimators that can serve as double checks and/or cross validation of the findings from the FPT. Such an advantage might prove invaluable especially for noisy data, and this is an asset to the main goals of the mentioned roadmap which is, therefore, not limited only to the FPT.

2.3. The dimensionality reduction problem within the Padé methodologies

Large scale computations for huge systems with enormous dimension/length and/or many degrees of freedom of the entry data to be analyzed/processed are customarily encountered in many important studies across inter-disciplinary

research including medicine, engineering and technology/industry. Invariably, such exceedingly difficult and mathematically ill-conditioned problems have been tackled with the iterative LA, first for an effective dimensionality reduction of the initial problem via Jacobi tri-diagonalization, and then for extracting the parametrized characteristics of the studied system. Alternatively, and advantageously, the dimensionality problem has recently been solved very efficiently both in the frequency and the time domain by means of the FD and DSD (or DLP, DPA) [1]. These parametric estimators employ windowing or beam-spacing to segment the initial large problem into a sequence of small problems in which only small well-conditioned matrices are diagonalized to extract the parametrized characteristics of the system. This segmentation is achieved by focusing on a part of the whole system's spectrum at a time without any loss of information by filtering out the remainder from the huge input data. The individual segments are subsequently inter-connected to cover the whole spectrum. Therefore, these powerful algorithms can alleviate severe ill-conditioning and permit accurate, reliable, robust and efficient reconstruction of the sought information from the entire system. Over the years, we used the LA, FD, DSD, DLP, DPA and other related algorithms in many applications in Nuclear Magnetic Resonance (NMR) [1], Ion Cyclotron Resonance Mass Spectroscopy (ICRMS) [1, 50]. It is our hope that a similar practice will be pursued also by other researchers, since the dimensionality problem is the bottleneck of all the other methods used in the MR literature and beyond.

In some applications of NMR and MRS, it is necessary to go beyond the usual one-dimensional parametric estimations. To this end, the FPT can be used with confidence, since it automatically extends its applicability to multi-dimensional processing, as a truly coherent spectral analysis by treating all the variables simultaneously [2]. This is a great advantage relative to multi-dimensional FFT, which is a sequential processing in this case (one variable at a time) and, hence, inherently a non-coherent train of one-dimensional FFTs.

3. Theory of spectral analysis

3.1. Basic concepts on Padé rational responses to any external perturbation of systems

Signal and image processing developed autonomously and remained for a long time mainly within the realm of applied sciences as well as engineering. Yet, here, very similar methods have been used as in the basic sciences. In electric circuit theory, a frequently used method is the so-called rational response of the system to external perturbation [1]. This response is, in fact, the PA in the frequency domain. As mentioned, precisely the same type of PA can also be found in various fields that use signal processing (e.g. speech patterns, system

theory, optimizations, etc) or in mathematical statistics under different acronyms e.g. ARMA [1]. Many more opportunities might open up to further signal and image processing, as well as to provide new tools for studying generic spectra irrespective of their experimental or theoretical origins. This cross-fertilization is anticipated to have a twofold benefit in the emergence of new high-resolution signal/image processors for applied sciences as well as engineering and, in turn, for basic sciences when analyzing spectra of large physical, chemical or biological systems as well as living organs/species. The literature on signal and image processing in applied mathematics and engineering is abundant with specially designed methods for robust performance in industry and technology under rigorous requirements for accuracy, stability and reliability. To achieve such strict goals, the most advanced mathematical methods have been used. These could be exported to sciences for versatile applications. In order that such a practice is developed further in a systematic rather than a sporadic manner, this review encourages more cross-disciplinary interactions that could advantageously reduce duplication in non-overlapping fields.

Reconstructing spectra and images from the received signals is a general inverse problem with its intrinsic time development, which is ideally suited for description by the Schrödinger picture of quantum mechanics. Therefore, it could be beneficial for signal and image processing to intertwine with quantum-mechanical description of stationary and time-independent phenomena. It is only within recent years, as has thoroughly been reviewed in Ref. [1], that the situation improved through using quantum mechanics and quantum resonant scattering theory in signal processing, by relying upon the concept of auto-correlation functions as the amplitude probabilities for survival of the Schrödinger states of studied systems. In such an approach, the Schrödinger ordinary or generalized eigenvalue equations and the spectral problem of the resolvent or the Green operator play pivotal roles.

The polynomial quotient P_K/Q_K(diagonal) or P_{K-1}/Q_K (para-diagonal) as a rational function in e.g. harmonic variable $z^{-1} = \exp(-i\omega\tau)$, is known in the literature as the PA for the corresponding Maclaurin series in z^{-1}. In signal processing, the PA is alternatively called the fast Padé transform [37–39] to highlight the possibility of obtaining a shape spectrum from an FID via a non-parametric estimation as reminiscent of the FFT. The latter type of estimation is done by simply evaluating the Padé spectrum (e.g. P_K/Q_K) without ever searching for any of the spectral parameters that are the complex frequencies $\{\omega_k\}$ and amplitudes $\{d_k\}$. In other words, the FPT can compute the envelope spectrum without having to extract the spectral parameters $\{\omega_k, d_k\}$. This is in sharp contrast to e.g. HLSVD [45], which computes the envelope spectrum by first reconstructing the peak parameters $\{\omega_k, d_k\}$. Most importantly, the FPT can perform parametric estimations by rooting the polynomial Q_K whose roots $\{z_k^{-1}\}$ yield $\{\omega_k\}$ and this leads to $\{d_k\}$ for each resonance. For example, the para-diagonal FPT treats the exact spectrum, i.e. the mentioned Maclaurin sum which is in signal

processing equal to the finite-rank Green function $G_N(z^{-1})$, via the *unique* ratio of two polynomials $P_{K-1}(z^{-1})/Q_K(z^{-1})$ at *any frequency* ω:

$$G_N(z^{-1}) = \frac{1}{N}\sum_{n=0}^{N-1} c_n z^{-n}, \tag{2}$$

$$G_N(z^{-1}) \approx \frac{P_{K-1}(z^{-1})}{Q_K(z^{-1})} = \sum_{k=1}^{K} \frac{d_k}{z^{-1} - z_k^{-1}}, \tag{3}$$

$$P_{K-1}(z^{-1}) = \sum_{r=0}^{K-1} p_r z^{-r}, \quad Q_K(z^{-1}) = \sum_{s=0}^{K} q_s z^{-s}, \tag{4}$$

where $z = e^{i\omega\tau}$and $z_k = e^{i\omega_k\tau}$. In the FPT, the sum $\sum_{k=1}^{K} d_k/(z^{-1} - z_k^{-1})$ represents the complex-valued *total shape spectrum* (envelope) which is the sum of the K corresponding *component shape spectra*, $d_k/(z^{-1} - z_k^{-1})(1 \leqslant k \leqslant K)$. Here, P_{K-1} and Q_K are readily extracted from the input data G_N by treating the product $G_N Q_K$ in the defining relation $G_N Q_K = P_{K-1}$ as a convolution.

It should be noted that the FPT has its two variants denoted by FPT$^{(+)}$ and FPT$^{(-)}$ that have their initial convergence range inside ($|z| < 1$) and outside ($|z| > 1$) the unit circle, respectively. Being rational polynomials, both of these variants of the FPT extend automatically their applicability to the whole complex plane (inside as well as outside the unit circle) by recourse to the Cauchy principle of analytical continuation. The expansion variables in the FPT$^{(+)}$ and the FPT$^{(-)}$ are $z^{+1} = z$ and $z^{-1} = 1/z$, respectively. The complex-valued spectrum in the para-diagonal form within the FPT$^{(-)}$ is given in Eq. (3). Similar expressions exist for the FPT$^{(+)}$ [43, 44]. Interchangeably, the numerator and the denominator polynomials in the FPT$^{(+)}$ and the FPT$^{(-)}$ will have the plus and minus superscripts, $P_L^{\pm}$ and $Q_K^{\pm}$, where the degree L is usually equal to K or $K-1$ for the diagonal or para-diagonal FPT, respectively.

3.2. Determination of the exact number of resonances by the FPT

Recently, we have demonstrated [1,43,44] that the exact number $K$of resonances is extractable from the investigated time signal $\{c_n\}$ without the customary guessing used in the MRS literature. This is accomplished both in the time and the frequency domain. The time signal is usually stored as the Hankel or the so-called data matrix, $H_K(c_n)$. We have shown that the FPT exists if, in the time domain, the corresponding Shanks transform of order K is zero [1]. The

Shanks transform of order K, as denoted by $e_K(c_n)$, is proportional to a ratio of the two Hankel determinants:

$$e_K(c_n) \propto \frac{H_{K+1}(c_n)}{H_K(c_n)}. \tag{5}$$

Thus, the Shanks transform and the FPT exist if the following two conditions are simultaneously fulfilled:

$$H_K(c_n) \neq 0, \quad H_{K+1}(c_n) = 0. \tag{6}$$

In other words, the signature for the given signal to have precisely K resonances is detected whenever both conditions in (6) are satisfied. In practice, to verify (6), we compute recursively the sequence of Hankel determinants of increasing order $\{H_m(c_n)\}$ $(m = 1, 2, \ldots)$ [1]. The first integer $m' = m$ at which (6) is satisfied gives the total number of metabolites, $K = m'$. Moreover, if the time signal has exactly K damped exponentials, then on top of (6), the following relationship is also true:

$$H_K(c_n) \neq 0, \quad H_{K+m}(c_n) = 0 \quad (m = 1, 2, \ldots). \tag{7}$$

In other words, the zero-valued Shanks transform as per equation $e_{K+m}(c_n) = 0$ $(m = 1, 2, \ldots)$ is the signature for the time signal $\{c_n\}$ to have precisely K attenuated exponentials with stationary or non-stationary (polynomial type) amplitudes that yield non-degenerate (Lorentzian) or degenerate (non-Lorentzian) spectrum, respectively. We have shown in Refs. [1,42–44] that this procedure for obtaining K exactly from the raw time signal $\{c_n\}$ is fully applicable to MRS data.

In the frequency domain, we have developed another powerful procedure for determining K exactly, and that is accomplished through the so-called pole-zero cancellations [42–44]. This is achieved by computing a sequence of Padé spectra $\{P_m/Q_m\}$ $(m = 1, 2, \ldots)$ in a frequency range of interest or in the whole Nyquist range $[-\pi/\tau, \pi/\tau]$. In this procedure, the exact number K of resonances is determined when the following stability condition is detected:

$$\frac{P_{K+m}}{Q_{K+m}} = \frac{P_K}{Q_K} \quad (m = 1, 2, \ldots). \tag{8}$$

This is possible by means of a truly extraordinary phenomenon called pole-zero cancellations that is unique to the Padé polynomial quotients. The zeros of the numerator polynomial P_K are the zeros of the polynomial quotient P_K/Q_K in the FPT. Likewise, the zeros of the denominator polynomial Q_K are the poles of the same Padé quotient P_K/Q_K, because this latter rational function is a meromorphic function, as mentioned. When both polynomials P_{K+m} and Q_{K+m} are written in their canonical forms, i.e. via products of terms containing their respective zeros, then it is immediately apparent that Eq. (8) can be satisfied only

if all the zeros and poles of P_{K+m}/Q_{K+m} coincide with each other for m greater than 1, provided that the spectrum has exactly K resonances. This leads to cancellations of all these poles and zeros beyond the order K which, therefore, must be the sought exact number of resonances in the investigated frequency spectrum. The said cancellations reduce the ratio P_{K+m}/Q_{K+m} to P_K/Q_K for any positive integer m greater than unity, and this is precisely the content of Eq. (8). Moreover, we have shown that all the amplitudes of these cancelled pole-zero doublets are equal to zero [42–44]. In this way, by this indeed remarkable feature of the briefly outlined pole-zero cancellation, the FPT is safeguarded with fidelity against overestimating the true number K of resonances, since any other higher value $K + m$ ($m = 1, 2, \ldots$) will certainly give exactly the same spectral parameters and, therefore, the same spectra, as well as the same reconstructed time signals.

3.3. Unambiguous identification of overlapping genuine resonances by the FPT

We have shown that the FPT can identify spurious resonances by analytical methods; and how this is followed by a well-defined procedure for regularization, via the so-called constrained root reflection with preservation of the magnitude or power spectra [1]. Overlapping or hidden metabolites, including those that may be disguised as noise, are retrieved with fidelity [42–44]. In realistic synthesized models, we have illustrated that the FPT successfully identifies overlapping peaks that are entirely missed by the FFT [42–44].

3.4. Treatment of Lorentzian and Non-Lorentzian spectra on the same footing by the FPT

We have also shown in Refs. [1,27,41] that the FPT can treat both Lorentzian (non-degenerate) and non-Lorentzian (degenerate) spectra on the same footing. This is a distinct advantage of the FPT relative to the HLSVD [45] which is limited to Lorentzians only. Such a virtue of the FPT is very important, because overlapping resonances can be non-Lorentzian and they are abundant in MRS data. Moreover, as mentioned, overlapping resonances are often of utmost clinical relevance.

4. The quantification problem

4.1. Reliable extraction of complex frequencies and amplitudes by the FPT

In Refs. [31–44] we implement and benchmark the computational algorithms by which the FPT provides the peak parameters needed to quantify

metabolite concentrations in MRS. *This gives the unique and exact solution with no recourse to any fitting whatsoever* . Briefly, as stated, the complex spectrum in the FPT is defined by e.g. the polynomial quotient P_{K-1}/Q_K which naturally leads to peaks at the zeros of the denominator polynomial Q_K. Thus, root searching of Q_K gives the complex harmonic variables $z_k^{-1}(1 \leqslant k \leqslant K)$, so that the sought ω_k is deduced via $\omega_k = (i/\tau)\ln(z_k^{-1})$. The corresponding complex amplitudes $\{d_k\}$ are subsequently obtained from the analytical formula given by the Cauchy residue of the polynomial ratio in the FPT via $d_k = P_{K-1}(z_k^{-1})/Q'_K(z_k^{-1})$, where $Q'_K(z_k^{-1}) = dQ_K(z_k^{-1})/dz_k^{-1}$. Hence, the residue is evaluated only at one complex frequency ω_k yielding the sought d_k.This is highly advantageous relative to the HLSVD and other parametric estimators from MRS. In the HLSVD, all the found frequencies $\{\omega_m\}$ are used to compute a single d_k. As a consequence, any found spurious frequencies in the HLSVD would undermine the accuracy of the computed d_k. The actual computations of the amplitudes in the HLSVD are done by solving a system of linear equations as opposed to the analytical formula in the FPT. Thus, the FPT arrives at the spectral parameters $\{\omega_k, d_k\}$ with minimal computational effort and maximal accuracy. Here, the real $\{\mathrm{Re}(\omega_k)\}$ and the imaginary $\{\mathrm{Im}(\omega_k)\}$ part of ω_k are the position and the width of the k^{th} peak, whereas $\{|d_k|/\mathrm{Im}(\omega_k)\}$ and Arg (d_k) are the corresponding height and phase, respectively.[4] Specifically, the FPT can first find all the peak parameters of every physical metabolite *without ever using the Fourier or any other spectrum.* The Padé spectrum $\sum_{k=1}^{K} d_k/(z^{-1} - z_k^{-1})$ can be constructed afterwards in the absorption, dispersion, magnitude or power mode. Alternatively, the shape spectrum (i.e. the envelope of the peaks as reminiscent of the FFT) can be obtained in the FPT without computing the spectral parameters $\{\omega_k, d_k\}$ by simply evaluating the quotient $P_{K-1}(z^{-1})/Q_K(z^{-1})$ at any frequency ω where $\omega=(i/\tau)\ln(z^{-1})$. This is in contrast to all the other parametric methods, such as HLSVD, LP, FD and the like that compute the shape spectrum only through the Heaviside partial fraction representation $\sum_{k=1}^{K} d_k/(z^{-1} - z_k^{-1})$ which, obviously, necessitates the spectral parameters $\{\omega_k, d_k\}$. The FPT, as a polynomial quotient, is the signal processor which is the most adapted to the quantification problem in MRS. This is because the sought spectrum $\sum_{k=1}^{K} d_k/(z^{-1} - z_k^{-1})$ or $\sum_{k=1}^{K} d_k/(\omega - \omega_k)$ is, in fact, itself a ratio of two polynomials, $\sum_{k=1}^{K} d_k/(\omega - \omega_k) = P_{K-1}(\omega)/Q_K(\omega)$, precisely as in the definition of the FPT. Hence, for such problems, the FPT actually becomes *the exact theory* for spectral analysis of time signals comprised of damped complex exponentials whose amplitudes can be stationary and/or non-stationary (polynomial type) [1].

[4]Hereafter, $\mathrm{Re}(u)$ and $\mathrm{Im}(u)$ denote the real and imaginary parts of a complex number u.

4.2. Separation of genuine from spurious resonances by the FPT

Physical (genuine) and unphysical (spurious) resonances are disentangled through their diametrically opposite behaviors at different partial signal lengths $N/M(M > 1)$. Resonances whose spectral parameters retain their stability within a pre-assigned accuracy threshold at least for $N/2$ and N are classified as genuine, whereas if this is not the case, they are considered to be spurious. These latter spurious resonances are removed from the final list of reconstructed spectral parameters, so that only the genuine resonances are retained, as demonstrated in Ref. [42–44]. This, in turn, improves SNR in the final absorption spectra of the FPT.

4.3. Recapitulation of the main algorithmic aspects of signal processing within the FPT

Using the FPT to analyze the encoded FIDs, the coefficients $\{p_r, q_s\}$ of the polynomials P_{K-1} and Q_K are computed efficiently by solving the systems of linear equations deduced from definition (2), by treating the product in $G_N(z^{-1}) * Q_K(z^{-1}) = P_{K-1}(z^{-1})$ as a convolution [1,50]. Once all the pairs $\{p_r, q_s\}$ are obtained, the (non-parametric) envelope spectrum can be computed by evaluating the quotient $P_{K-1}(z^{-1})/Q_K(z^{-1})$ at any selected frequency ω, as discussed. To extract the peak parameters, one solves the characteristic equation $Q_K(z^{-1}) = 0$. This latter polynomial equation has precisely K unique roots $z_k^{-1}(1 \leqslant k \leqslant K)$ and this yields the reconstructed fundamental frequencies ω_k from the already quoted relationship $\omega_k = (i/\tau)\ln(z_k^{-1})$. A similar procedure applies to the diagonal FPT, i.e. P_K/Q_K. Peak assignments can be made according to the most accurate available *in vitro* data from e.g. Refs. [20,24,51,52]. For reliable quantifications in MRS, it is not only the peak positions $\mathrm{Re}(\omega_k)$ that count, because the peak widths $\mathrm{Im}(\omega_k)$ and the complex amplitudes d_k are also critical. This is due to the fact that the k^{th} metabolite concentration is computed from the reconstructed peak parameters. From the spectral parameters, one can deduce the peak area underneath each resonance. Peak area is proportional to the concentration of the metabolite, relative to a selected reference concentration (water or another metabolite). Therefore, even for accurately determined ω_k's, the problem of obtaining the precise estimates of the d_k's becomes extremely important. In the FPT, the k^{th} amplitude d_k depends only upon the k^{th} root z_k^{-1} and it is obtained analytically from the Cauchy residue theorem [1]. Moreover, unlike guessing in the HLSVD [45] and in all the fitting algorithms from MRS [46–48], the FPT determines the true number K of resonances exactly, by e.g. the concept of Froissart doublets (pole-zero cancellations) [42–44]. Overall, the FPT completely avoids fitting and accomplishes accurate quantification by reliably extracting the parameters of all the physical metabolites directly from the raw encoded

FID. Specifically, when used as a parametric estimator, the FPT first finds all the peak parameters $\{\omega_k, d_k\}$ $(1 \leqslant k \leqslant K)$ of every physical resonance *without ever using the Fourier spectrum*, or any other spectrum. A spectrum can be constructed subsequently for e.g. visualization purposes, in any of the desired modes (absorption, dispersion, magnitude, power, etc). On the computational side, our MATLAB and C++ user-friendly software based upon the FPT, automatically performs the entire quantification of raw encoded FIDs in a very efficient way using only the standard programming. This software can be created as a portable module to be mounted as an interface to clinical scanners for widespread use in hospitals. Regarding the usage of the computer time, when implemented with the Euclid algorithm, the FPT scales like $N\ (\ln_2 N)^2$ with the signal length N [53, 54] for $N = 2^m$ $(m = 1, 2, 3, \ldots)$. This is of comparable efficiency to the FFT which scales as $N\ \ln_2 N$. However, as opposed to the FFT, it is pertinent to re-emphasize here that the FPT provides quantification *en route. Additionally, and this is what sets the Padé methodology apart from all the other parametric processors, the FPT possesses the analytical formulae for the entire spectral analysis in the most general case for any number of damped complex exponentials in the investigated time signal [1]. This overrides the notorious ill-conditioning of the quantification problem which is an inverse, mathematically ill-posed problem. Such a gold standard represents the most stringent test for the alternative numerical algorithms.*

After having applied the FPT to *in vivo* MRS FIDs encoded from patients with cancers and comparing this to the corresponding normative data, we suggest performing statistical multivariate analysis to determine the best set of metabolic predictors of malignancy, on a tumor-specific basis, using the results of quantification by the FPT. Further, we plan to develop data bases for non-malignant lesions that have presented differential diagnostic dilemmas, notably benign tumors, infectious or inflammatory lesions. For the breast, e.g. these non-malignant lesions include ductal hyperplasia, fibroadenoma, fibrocystic changes, as well as lactating breast. We will use multivariate analysis to determine the best set of metabolic predictors of malignancy as opposed to benign pathology. This latter step is of crucial importance for improving the specificity of MRS and MRSI with respect to cancers.

5. Most recent results

5.1. Exact quantification in MRS by the FPT for theoretically synthesized FIDs

Confidence in the FPT is built systematically by considering synthesized and encoded FIDs. For noise-free synthesized FIDs, the FPT returns all the spectral parameters (irrespective of their number) within machine accuracy [42–44, 50]. For noise-corrupted simulated FIDs, all the known physical spectral parameters are retrieved by the FPT with 3–4 accurate digits for SNRs of the

level typically encountered in time signals encoded via MRS [43]. This latter high level of accuracy is also consistently maintained when the FPT is applied to FIDs encoded via MRS, as documented in our most recently published studies [27,40,41]. Although our initial studies on MRS [27,40,41] have focused on envelope spectra, we nevertheless carried out quantifications. Such an occurrence can be understood from the fact that these latter envelope spectra [27,40,41] have been generated from the Heaviside partial fraction representation (3) which relies exclusively upon the reconstructed fundamental frequencies and the corresponding amplitudes as the key parameters for quantification.

We begin by presenting our results on spectra that correspond to a theoretically generated (synthesized) FID which is reminiscent of time signals typically encoded clinically from a healthy human brain via MRS using an external static field $B_0 = 1.5$ T and a short TE of about 20 ms, with total length $N = 1024$ and bandwidth 1000 Hz so that $\tau = 1$ ms (see e.g. [55]).

Table 1 gives the results of exact quantification via parametric spectral analysis within the FPT. Shown are all the physical parameters of each of the 25 reconstructed resonances. For every peak, these retrieved physical quantities include complex fundamental frequencies and the corresponding amplitudes that yield the position, width, height and phase of the given resonance (all the phases are set to equal zero in the input FID, $d_k = |d_k| \exp(\varphi_k) = |d_k|, \varphi_k = 0, 1 \leqslant k \leqslant 25$). Such findings permit extraction of other physical quantities in terms of which both the FID and its spectrum are *clinically* interpreted. These are the transverse relaxation times T_2 and concentrations of each metabolite.[5] With this, the clinical relevance of an estimator, which like the FPT can reliably reconstruct concentrations of metabolites from encoded FIDs, becomes evident. As seen in Table 1, the input spectral parameters are given with 4 digits of accuracy. Remarkably surpassing this latter level of precision, in Refs. [43] and [44], the input spectral parameters have been defined with 12 digits of accuracy, but still the ensuing reconstructions by the FPT were exact.

From the unequivocally reconstructed spectral parameters, we can generate the component spectra for every physical resonance. In Refs. [42–44], using noise-free and noise-corrupted synthesized FIDs, we demonstrate that using at most one quarter ($N/4 = 256$) of the full signal length ($N = 1024$), the FPT can fully resolve and quantify all the constituent resonances, including those that are isolated, overlapped, tightly overlapped as well as nearly degenerate. These

[5]A metabolite being a molecule can be associated with more than one resonance. Physically, using ^{1}H MRS, concentration for a given chemical shift is proportional to the intensity of the corresponding metabolite signal. This latter intensity itself is proportional to the total number of protons that resonate at a given chemical shift. Chemical shifts vary from one compound to another depending upon the extent of electronic shielding of the external static magnetic field strength B_0. Although very small, this shielding of B_0 is the very reason for the existence of MRS. In this way, the concentrations of metabolites reveal the molecular compounds into which the resonating protons are bound.

Table 1
Converged Padé-reconstructed spectral parameters and concentrations of 25 resonances using only 220 FID points in the FPT$^{(-)}$.

Peak #	Assignment	$\mathrm{Re}(f_k^-)$ (ppm)	$\mathrm{Im}(f_k^-)$ (ppm)	$\lvert d_k^- \rvert$ (au)	Concentration (mMol/ww)	Fraction
1	Mobile Lipids	0.985	0.180	0.122	7.930	0.71
2	Mobile Lipids	1.112	0.257	0.161	10.465	0.94
3	Mobile Lipids	1.548	0.172	0.135	8.775	0.79
4	Mobile Lipids	1.689	0.118	0.034	2.210	0.20
5	GABA	1.959	0.062	0.056	3.640	0.33
6	N-Acetyl Aspartate (NAA)	2.065	0.031	0.171	11.115	1.00
7	NAAG	2.145	0.050	0.116	7.540	0.68
8	GABA	2.261	0.062	0.092	5.980	0.54
9	Glutamate (Glu)	2.411	0.062	0.085	5.525	0.50
10	Glutamine (Gln)	2.519	0.036	0.037	2.405	0.22
11	Aspartate (Asp)	2.675	0.033	0.008	0.520	0.05
12	NAA	2.676	0.062	0.063	4.095	0.37
13	Asp	2.855	0.016	0.005	0.325	0.03
14	Creatine (Cr)	3.009	0.064	0.065	4.225	0.38
15	Phosphocreatine (PCr)	3.067	0.036	0.101	6.565	0.59
16	Choline (Cho)	3.239	0.050	0.096	6.240	0.56
17	Phosphoryl choline(PCho)	3.301	0.064	0.065	4.225	0.38
18	Taurine (Tau)	3.481	0.031	0.011	0.715	0.06
19	Myoinositol (M-Ins)	3.584	0.028	0.036	2.340	0.21
20	Glu	3.694	0.036	0.041	2.665	0.24
21	Gln	3.803	0.024	0.031	2.015	0.18
22	Cr	3.944	0.042	0.068	4.420	0.40
23	PCr	3.965	0.062	0.013	0.845	0.08
24	PCho	4.271	0.055	0.016	1.040	0.09
25	Water	4.680	0.136	0.113	7.345	0.66

Here, the quantity 'fraction' is defined as C_{met}/C_{NAA}, where C_{met} and C_{NAA} are the concentrations of the given metabolite and that of NAA, respectively. All the listed assignments of the reconstructed metabolites in this table have been made according to the data base from Ref. [51].

recent studies [42–44] represent a veritable paradigm shift for signal processing in MRS with particular relevance to clinical oncology, due to the unprecedented capability of the FPT to unambiguously resolve and quantify all the physical resonances. This is presently illustrated for noiseless FIDs in figures 1 and 2.

Figure 1 shows the way in which the complex frequencies (left column) and the absolute values of the amplitudes (right column) are retrieved by the FPT$^{(-)}$ at FID lengths N_P = 180, 220 and 260. It is seen that convergence is attained for both of these spectral parameters at N_P = 220 for all the 25 resonances.

In figure 2, we display the component and total spectra. Each resonance is seen to have its spectrum, i.e. the component spectrum $d_k^-/(z^{-1}-z_k^{-1})$. The sum of all the component spectra gives the total shape spectrum $\sum_{k=1}^{K} d_k^-/(z^{-1}-z_k^{-1})$, or equivalently, the envelope spectrum (right column) at a fixed partial signal length. This figure shows how a given total shape spectrum is built from the corresponding component spectra. Illustrations are depicted for three partial lengths N_P=180, 220 and 260 of the full FID. The FPT component spectra are seen in figure 2 to reach full convergence at $N_P = 220$. These latter component spectra from panel (ii) remain unaltered at N_P>220 as shown on panel (iii) for $N_P = 260$. The same is true for the total shape spectra (panels v and vi). The most striking feature of figure 2 is that even at $N_P = 180$, the total shape spectrum (panel iv) has reached full convergence despite the lack of stability of some of the corresponding component spectra (panel i). Namely, when passing from $N_P = 180$ (panel i) to $N_P = 220$ (panel ii) a new resonance #11 at 2.675 ppm is detected as a near degeneracy with its closely neighboring peak #12 at 2.676 ppm. Here, chemical shift splitting between peaks #11 and #12 is only 0.001ppm (see also Table 1). Resonance #12 for $N_P = 180$ is over-estimated, such that its peak area is enhanced precisely by the amount of the missing peak #11. Moreover, the so-called residual or error spectrum of the envelope spectrum[6] for N_P =180 does not indicate the absence of peak #11. However, the component spectra require N_P=220 in order to detect and accurately quantify peak #11. This illustrates the non-reliability of a given total shape spectrum when it is used to reconstruct the constituent component spectra and their peak parameters, as is actually done in attempts to quantify via all the fitting recipes in MRS [46–48].

We now compare in figure 3 the performance of the FPT and the FFT for absorption total shape spectra. Here, the resolution and convergence rates are clearly seen to be much better in the FPT than in the FFT at any partial signal length $N_P = N/M (M > 1)$. Especially striking is that already at $N/8 = 128$, the FPT quite closely reflects the shape of most of the converged spectrum. On the other hand, for the same fraction $N/8$ = 128, the FFT is unable to distinguish between choline and creatine around 3 ppm and, moreover, the four resonances within 3.5 – 4 ppm appear as a broad and uninterpretable bump. The FPT$^{(-)}$ is seen to converge at $N/4$ = 256 (panel vi) and this remains unaltered at $N/2$ = 512 and

[6]A residual (or error spectrum) in the FPT$^{(-)}$ is defined by the difference Re(F)[N] – Re(P_K^-/Q_K^-)[N_P] where the numbers in the square brackets indicate the FID lengths used in the absorption Fourier and Padé spectra Re(F) and Re(P_K^-/Q_K^-), respectively.

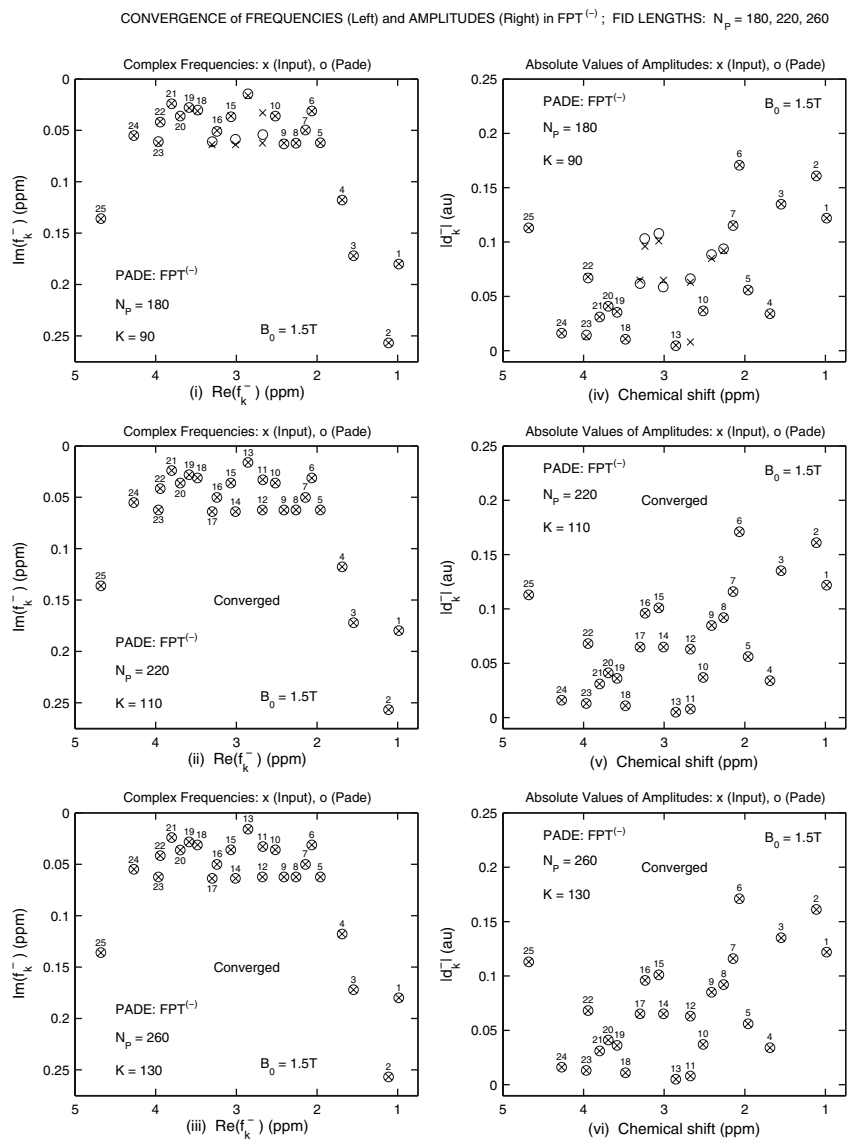

Figure 1. Distribution of the input as well as reconstructed frequencies and amplitudes. Convergence of the reconstructed spectral parameters of the FPT$^{(-)}$ is displayed at three partial FID lengths (N_P= 180, 220 and 260). The full FID length is N =1024. Throughout, spectral parameters $\{\omega_k, d_k\}$ from the FPT$^{(-)}$ are denoted as $\{\omega_k^-, d_k^-\}$, where $\omega_k^- = 2\pi f_k^-$and f_k^- is the linear frequency. Notice that unlike the FFT, the FPT can use any partial signal length, and not just the FIDs whose length is a special composite number, such as $2^m (m = 1, 2, \ldots)$. Hereafter, acronyms ppm and au abbreviate parts per million and arbitrary units, respectively.

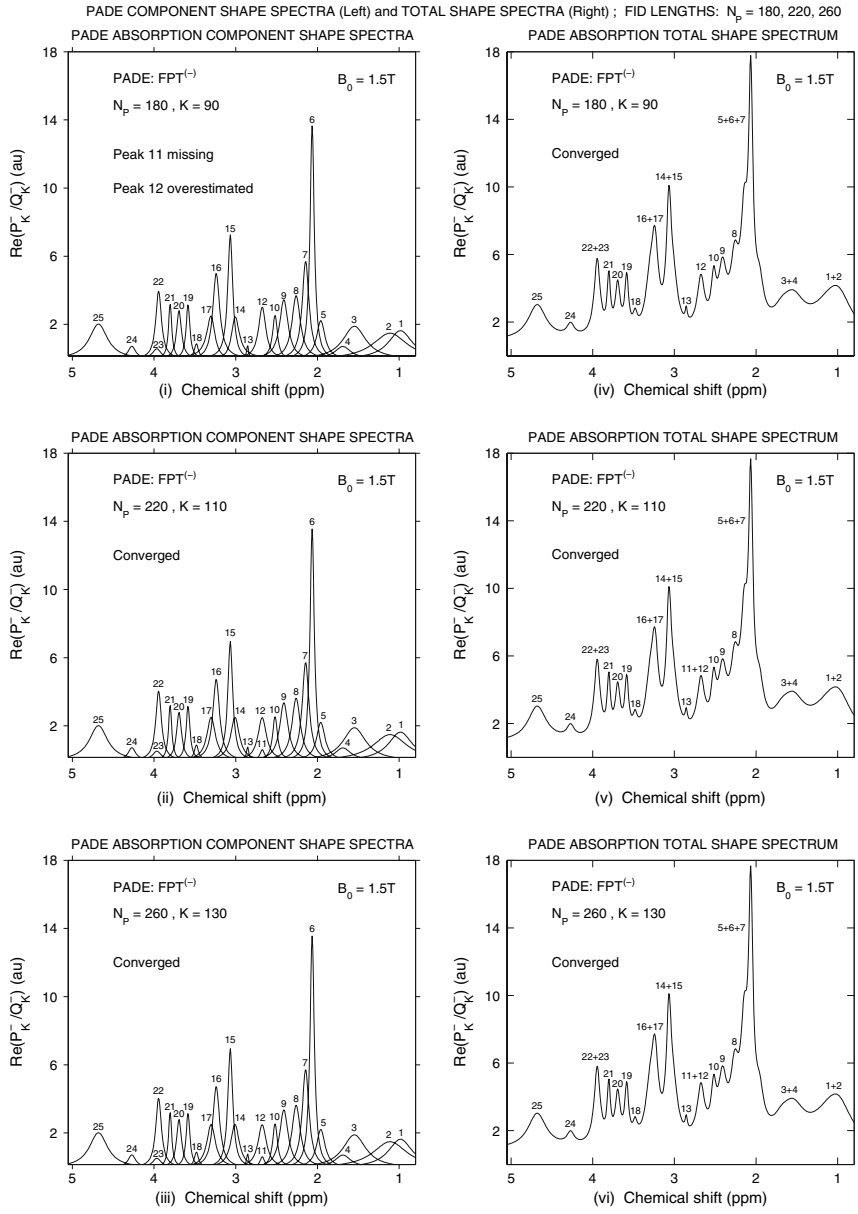

Figure 2. Absorption component shape spectra in $\mathrm{FPT}^{(-)}$ for each resonance (left) and their sums as total shape spectra (right). Displayed results correspond to three different partial signal lengths $N_P = 180$, 220 and 260. Total shape spectra at $N_P = 180$ on panel (iv) converge despite the missing peak #11, and the related overestimate of peak #12.

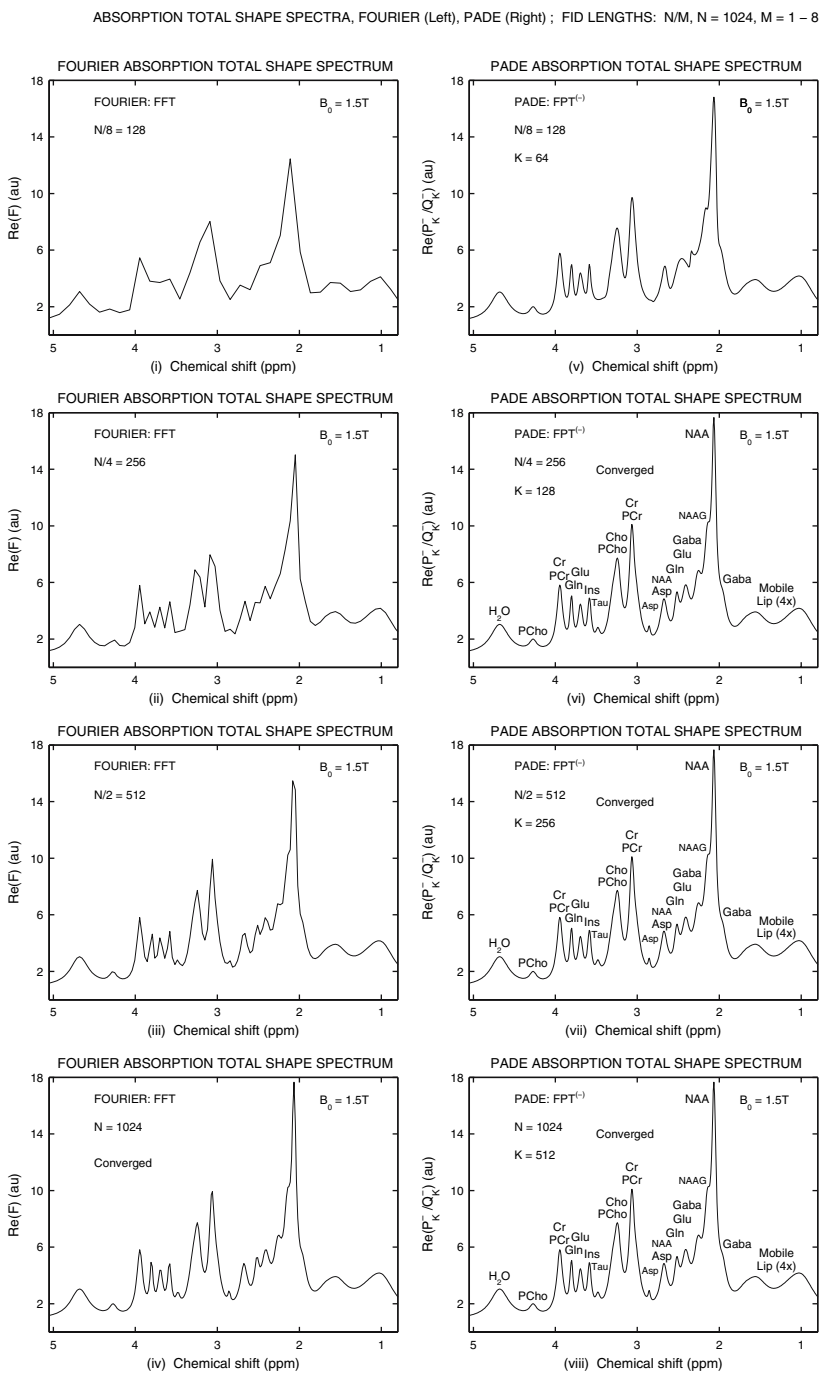

Figure 3. Convergence of absorption total shape spectra computed by the FFT (left) and the $\mathrm{FPT}^{(-)}$(right) using four different signal lengths ($N/8 = 128$, $N/4 = 256$, $N/2 = 512$ and $N = 1024$).

$N = 1024$ (panels vii and viii) by virtue of Froissart doublets or pole-zero cancellations, as per Eq. (8). By contrast, the FFT converges only after exhausting the full FID ($N = 1024$, panel iv).

5.2. *Stable and rapid convergence of the FPT for experimentally encoded FIDs*

Initially, performance of the FPT has been assessed in Ref. [32] for multiple numerical integration (quadratures) that are commonly encountered in MR physics. Therein, it was demonstrated that the FPT greatly accelerates convergence (with increasing number of sampling points) and yields unprecedented accuracy within *12 decimal places* using only $N = 512$ or 1024 points relative to only *2 decimal places* in the FFT. Combined with its robustness and stability, it was anticipated in Ref. [32] that the FPT will become the method of choice for MRS, MRSI as well as MRI which is a two-dimensional quadrature. The evidence of such an expectation from Ref. [32] has indeed become available in a series of most recent studies [1,2,6,7,18,19,27,31–44,49,56].

The above-quoted high accuracy in quadratures from Ref. [32] should translate directly into an increased resolution for quantification problems in MRS. Indeed, in Refs. [27,40,41] on quantification in MRS at 4T and 7T, it has been shown that, for partial signal length $N/M (M > 1)$, the clinically relevant resonances determining concentrations of metabolites in the investigated tissue are significantly better resolved in the FPT than in the FFT. In particular, it is verified that the FPT can achieve the same resolution as the FFT by using twice shorter time signals. As an illustration, this is also shown here for 4T in figures 4 and 5.

Error analysis is a key prerequisite for validity and usefulness of all parametric methods. This is illustrated in figure 6, which shows the so-called consecutive difference spectra as a proper measure of the error diminishing with increasing number of FID points used in reconstructions. The left column presents three consecutive difference spectra given by $\mathrm{Re}(P_K^-/Q_K^-)[N/32] - \mathrm{Re}(P_K^-/Q_K^-)[N/64]$, $\mathrm{Re}(P_K^-/Q_K^-)[N/16] - \mathrm{Re}(P_K^-/Q_K^-)[N/32]$ and $\mathrm{Re}(P_K^-/Q_K^-)[N/8] - \mathrm{Re}(P_K^-/Q_K^-)[N/16]$, where $N/64 = 32$, $N/32 = 64$ and $N/16 = 128$. The right column displays the further three consecutive difference spectra defined by $\mathrm{Re}(P_K^-/Q_K^-)[N/4] - \mathrm{Re}(P_K^-/Q_K^-)[N/8]$, $\mathrm{Re}(P_K^-/Q_K^-)[N/2] - \mathrm{Re}(P_K^-/Q_K^-)[N/4]$ and $\mathrm{Re}(P_K^-/Q_K^-)[N] - \mathrm{Re}(P_K^-/Q_K^-)[N/2]$, where $N/4 = 512$, $N/2 = 1024$ and $N = 2048$. These six sub-plots of intrinsic error spectra demonstrate a steady decrease of the local error in the $\mathrm{FPT}^{(-)}$ when the number of signal points are systematically augmented. Of course, error spectra that concern the $\mathrm{FPT}^{(-)}$ can also be generated by reference to other estimators e.g. the FFT. Likewise, the error spectra can be constructed by using the two variants of the FPT as done on the right columns of figure 7 showing the three residuals that are all related to the whole FIDs ($N = 2048$): $\mathrm{Re}(F)[N] - \mathrm{Re}(P^+/Q^+)[N]$(top panel), $\mathrm{Re}(F)[N] - \mathrm{Re}(P^-/Q^-)[N]$ (middle panel) and $\mathrm{Re}(P^+/Q^+)[N] - \mathrm{Re}(P^-/Q^-)[N]$ (bottom

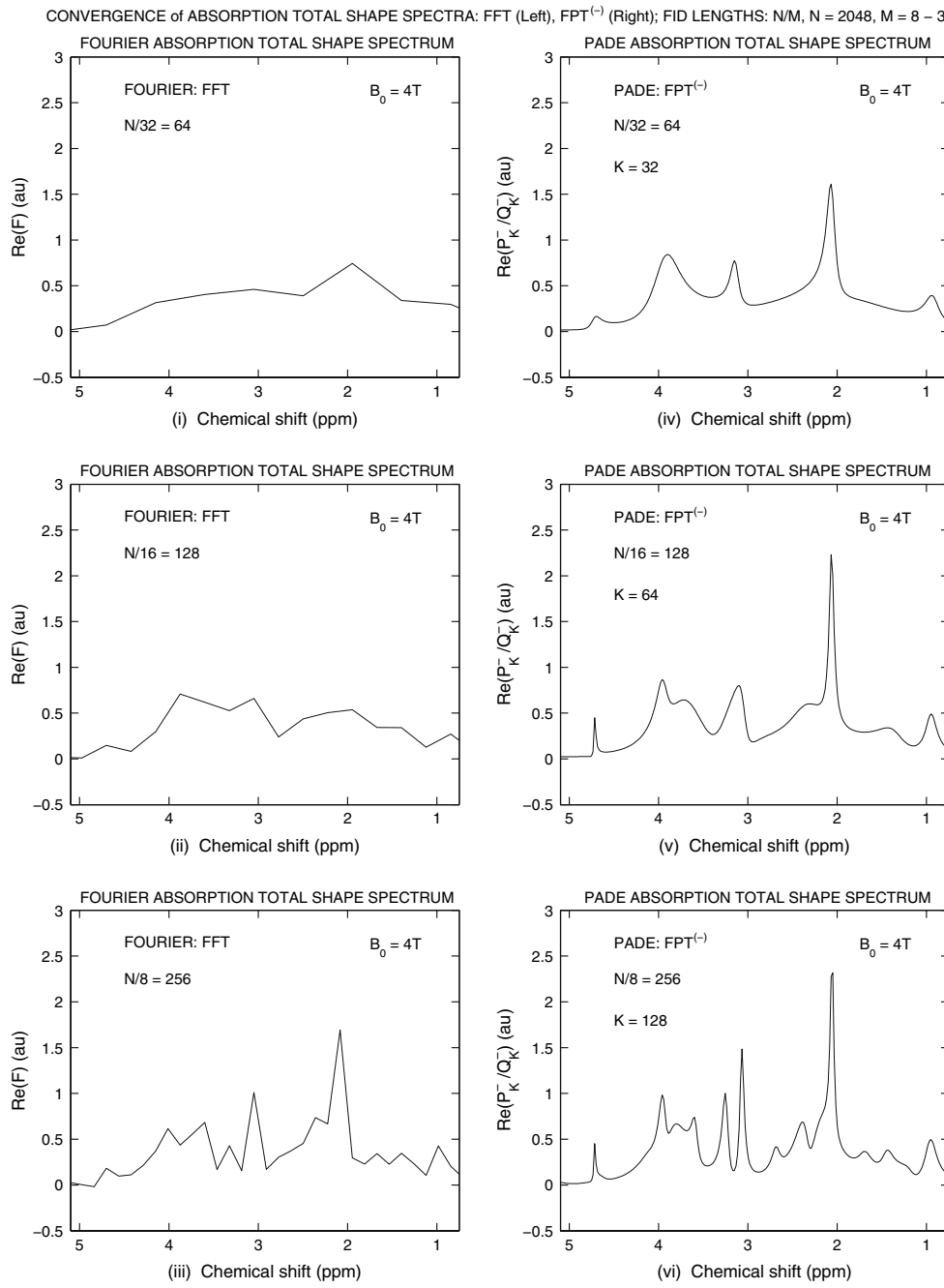

Figure 4. Fourier and Padé absorption spectra computed using 3 partial signal lengths ($N/32 = 64$, $N/16 = 128$, $N/8 = 256$) of the full FID ($N = 2048$, bandwidth = 6001.5 Hz) which has been encoded by Tkáč et al. [57] at 4T from occipital grey matter of a healthy volunteer.

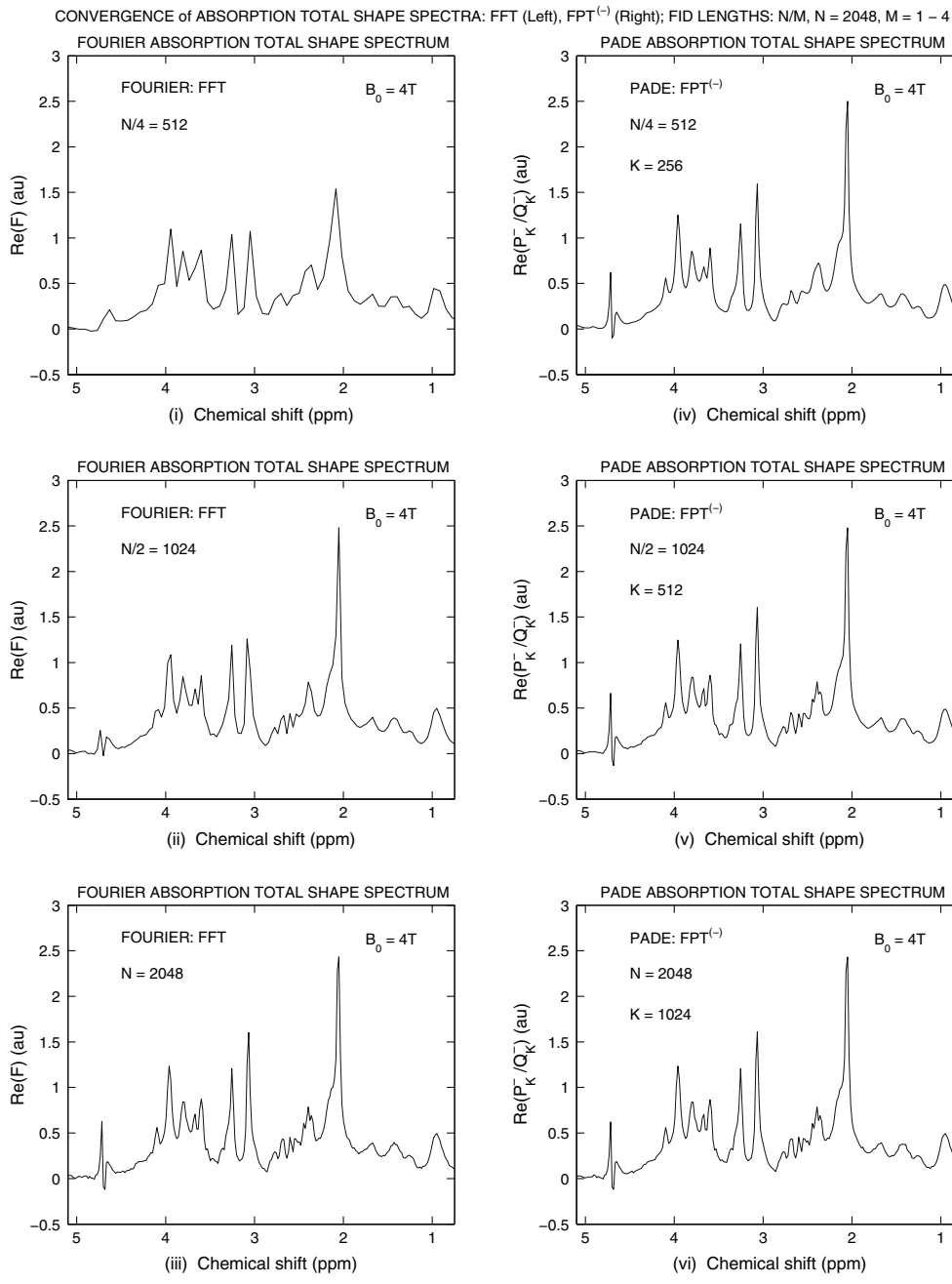

Figure 5. Fourier and Padé absorption spectra computed using 2 partial signal lengths ($N/4 = 512$, N/2 = 1024) and the full signal length $N = 2048$ which has been encoded by Tkáč et al. [57] at 4T from occipital grey matter of a healthy volunteer.

panel). All the three latter error spectra are seen to be indistinguishable from the background noise. Of particular importance are the entirely negligible values of the whole residual spectrum $\mathrm{Re}(P^{+}/Q^{+})[N] - \mathrm{Re}(P^{-}/Q^{-})[N]$ at any of the considered frequencies displayed on the right bottom panel of figure 7. This is a very important internal cross-validation within the FPT itself showing that its two variants, the $\mathrm{FPT}^{(+)}$ and the $\mathrm{FPT}^{(-)}$ are sufficient for establishing consistency of this processor without necessitating external checking against e.g. the FFT or other estimators.

Thus, as shown in figure 7, self-contained verification of all the results from the FPT is secured by using systematically both its variants, the $\mathrm{FPT}^{(+)}$ and the $\mathrm{FPT}^{(-)}$. The converged spectra from the $\mathrm{FPT}^{(+)}$ and the $\mathrm{FPT}^{(-)}$ are found to coincide within the experimental background noise level, and this represents one of the intrinsic cross-validations of the findings and robust error analysis of the FPT without relying upon the FFT or any other estimator [27,41].

6. Discussion

In this review, we address several critical issues related to resolution enhancement in signal and image processing of encoded biomedical data. These issues are of key relevance to such important public health problems as timely cancer diagnostics, screening, dose planning and treatment follow-up, as well as monitoring of radiotherapy. Resolution improvements are essential for adequate interpretation of data from patients and, hence, to clinical decision-making. Insufficient accuracy of all the existing Fourier-based algorithms that are commercially available and built into clinical scanners hampers progress, especially in diagnostic modalities based upon MRS and MRSI. Such a drawback stems from the time-bandwidth bound (the Rayleigh bound) which is inherent in Fourier methods and which limits resolution. Resolution is the weakest feature of the FFT and other methods are not sufficiently reliable and robust for short length noisy data records and overlapping spectral structures. Such obstacles can be overcome through *a paradigm shift* which was recently introduced into the MR research fields through an entirely novel strategy based upon the Padé methodology. In particular, the FPT identifies with fidelity the system's parameters as the poles and zeros of the system's response function extracted directly and accurately from the encoded data that are noisy and abundant with overlapping resonances. This critical feature, coupled with automated user-friendly software implemented *in situ* via protocols for conventional scanners, will facilitates enormously the clinician's adequate interpretation of the data encoded from patients. This is of paramount importance, since currently the wealth of biochemical information on metabolic functionality of the examined tissue is virtually unexplored by MRS, and thus limited mainly to the anatomical insight given by MRI. With this achievement through the FPT, it is envisaged that MRS and MRSI will finally make their way to hospitals and thus become routine clini-

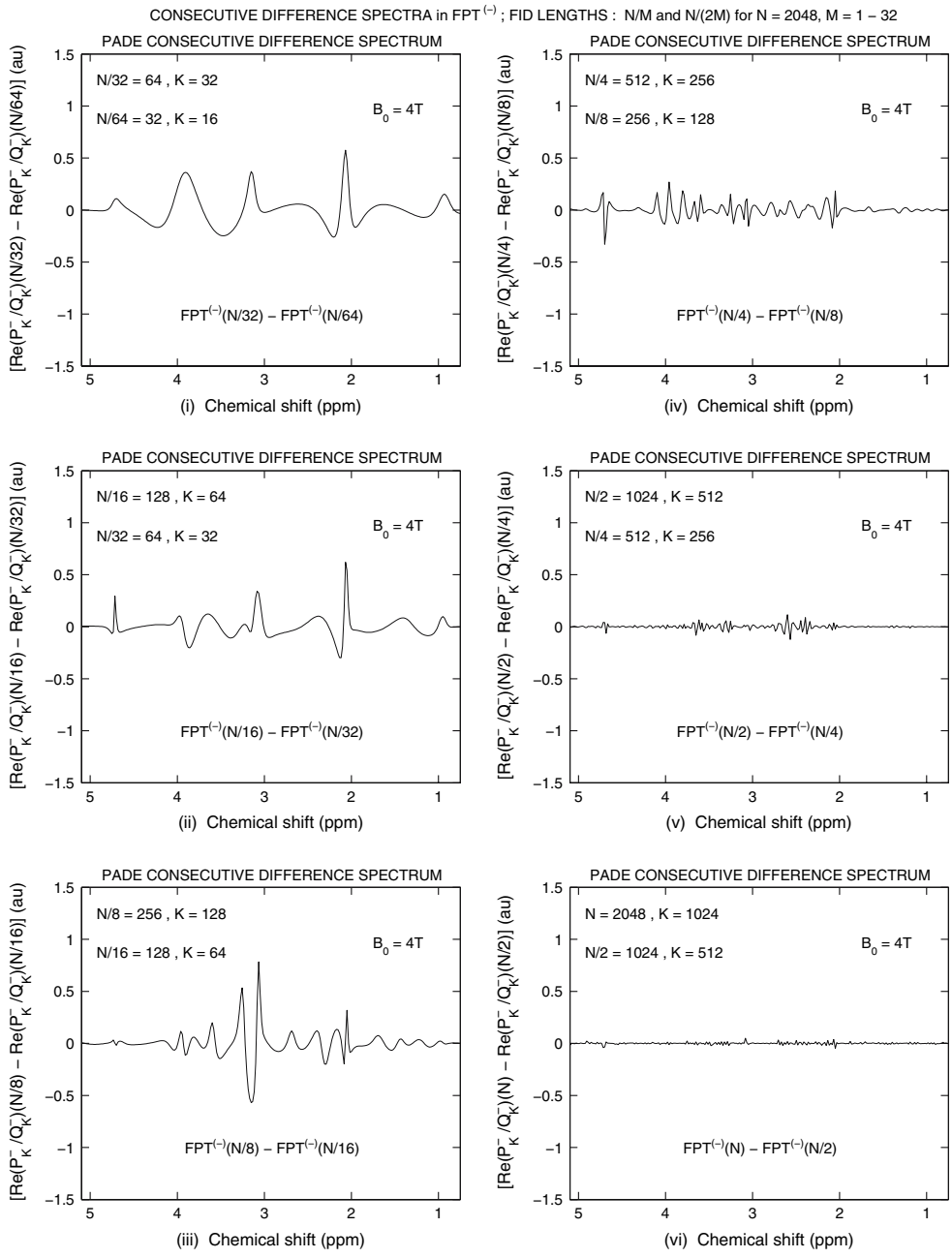

Figure 6. Consecutive difference spectra at 4T for absorption total shape spectra from the $FPT^{(-)}$at varying signal length, $N/64 = 32$, $N/32 = 64$, $N/16 = 128$, $N/8 = 256$,$N/4 = 512$, $N/2 = 1024$ and the full signal length $N = 2048$.

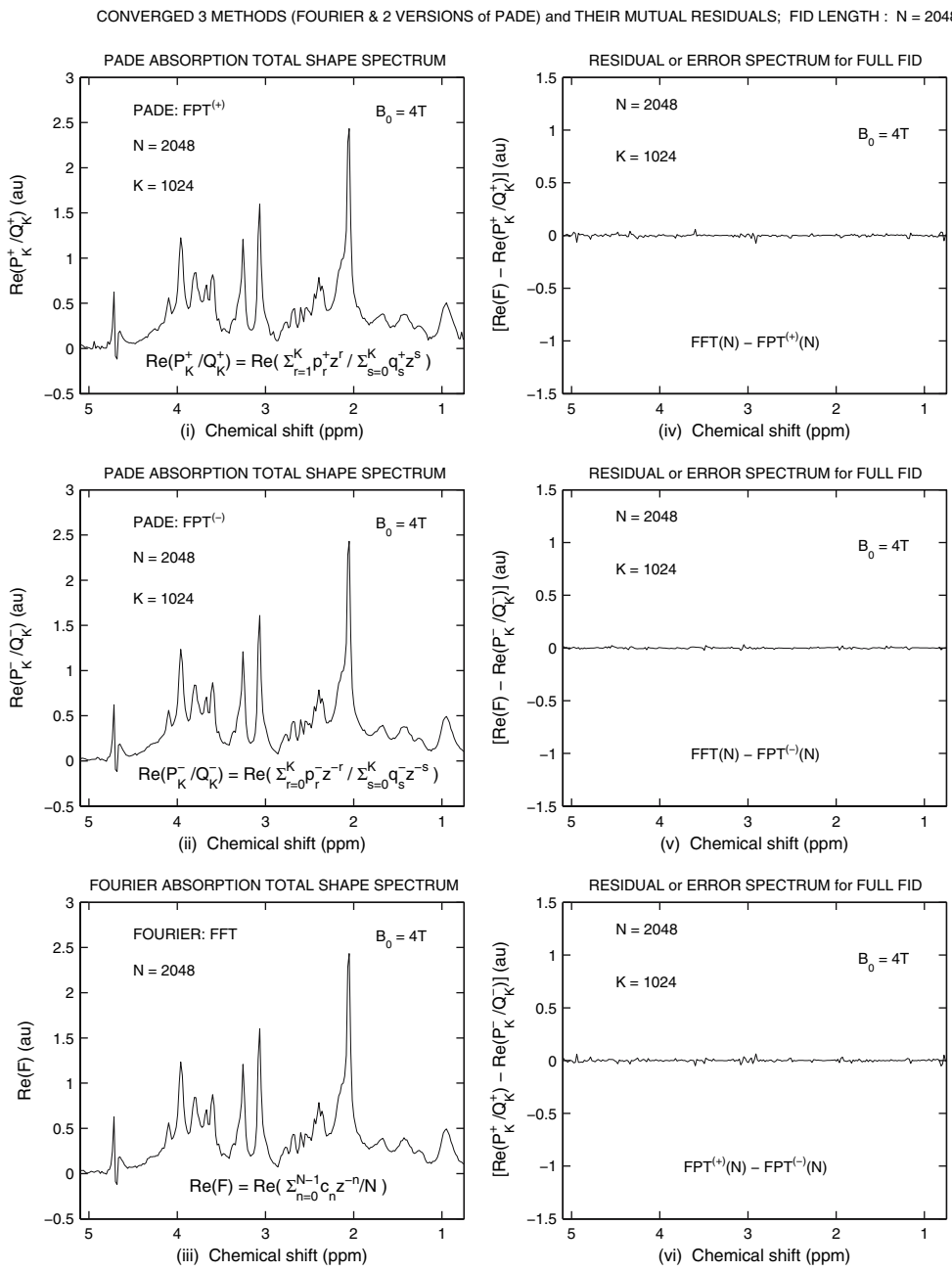

Figure 7. The absorption total shape spectra at 4T for full signal length ($N = 2048$) are shown on the left column for the $\mathrm{FPT}^{(+)}$ (top panel), the $\mathrm{FPT}^{(-)}$ (middle panel) and the FFT (bottom panel). The right column shows the residual absorption total shape spectra for the full FID: top panel (FFT – $\mathrm{FPT}^{(+)}$), middle panel (FFT – $\mathrm{FPT}^{(-)}$) and bottom panel ($\mathrm{FPT}^{(+)}$ – $\mathrm{FPT}^{(-)}$).

cal tools of a tremendous benefits to patients. Due to its unmatched reliability, robustness, error analysis, accuracy, enhanced resolution and efficiency, the FPT is bound to merge to MR technology and industry.

There is more to the FPT than MRS and MRSI that are the main theme of this review. The overall scientific thrust of the present study comes from the need for a unifying objective framework which intertwines in one whole the Padé-optimized signal/image processing with mathematically tailored data acquisition armamentarium, computer-based decision support and the control by the end user. The end-user for the medical/clinical purposes is the physician, but the outlined strategy is common to many similar problems in vastly different fields in sciences, engineering, technology and industry (metrology, speech processing, pattern recognition, mobile communication technologies, to name only a few). For example, metrology in health care devices and instrumentation is in need of methods and principles that can improve time- and space-resolution characterization as well as localization of chemical interactions on a sub-cellular and molecular level of the investigated tissue. This, as a very important spin-off from the presently outlined strategy, can be provided by the FPT.

Additionally, it is important to realize that the analyzed signal processing methods can be of direct use also to data acquisition. This can be accomplished by designing new sequence encodings that are tailored not to the FFT, as done in commercial scanners, but to the FPT. Such a novel vision is justified by the capability of the FPT to handle data with short echo times that can enhance the extraction of the information from the more insightful data due to the presence of clinically relevant short-lived metabolites. With this latter strategy, the borderline between data encoding and data analysis will become elusive, merging the two parts into a unified framework. This, in turn, would sharpen the request for more accurate experiments, thus making a natural bridge of the expounded signal processing avenues to high-precision measuring techniques from physics and chemistry in the medical setting, as suggested by the present review.

7. Conclusions and outlooks

7.1. Significance of MR physics for oncology

It is stunning that progress in imaging for cancer diagnostics, surgical therapy, radiotherapy, therapy planning and target definition relies heavily upon further fundamental advances within the three MR-based clinical tools: MRI, MRS and MRSI [58–63]. This is especially due to the potential of MRS and MRSI to provide detailed metabolic information on molecular and bio-chemical levels with superior *specificity* for a steadily increasing number of clinical applications, ranging from diagnosis to tumor treatment. Distinctly improved specificity of MRS and MRSI over other imaging techniques for e.g. diagnosis of tumor and other neoplastic diseases stems from the possibility of yielding *quantitative*

information on the investigated tissue. Moreover, such information is multifaceted and could be extracted through various clinically relevant parameters e.g. concentrations of tissue metabolites, relaxation times, chemical shifts, etc. By means of these parameters, the functionality of the examined tissue can be characterized in such great detail as to reveal the physical state and chemical bonds of tissue molecules that are the carriers of the resonating magnetic nuclei. Furthermore, it is especially important to emphasize that this is achieved in a completely non-invasive manner, i.e. without disrupting any of the physiological and metabolic functions of the tissue. This is the case because magnetic resonance leads to an extremely small energy dissipation in the tissue, far below the threshold needed for the damage of any living cell.

MRS and MRSI can revolutionize both diagnostics as well as therapy, and surpass the conventional anatomical/morphological information from MRI by providing a needed deep molecular insight into the scanned tissue. As a key to overall strategy of cancer treatment, early *tumor detection* by MRS and MRSI is potentially superior to MRI. This is due to two major factors: (i) improved specificity and (ii) detection of molecular changes prior to anatomical manifestation of the emergence and progression of the disease. Moreover, due to its full volumetric coverage of the investigated tissue, MRSI as a combination of MRI and MRS, can improve substantially a number of diagnostic and therapeutic strategies in clinical oncology, thus opening novel avenues in radiotherapy, chemotherapy and surgical oncology.

Such possibilities stem from a better delineation of target lesions and tumor boundaries by MRI (as automatically shared by the MRSI) than by other oncological non-MR-based imaging techniques. This superior target definition is secured by an excellent sensitivity of MRI to detect pathology, and such a property is imported into MRSI, which is a hybrid of MRI and MRS. A high sensitivity of MRI to depict pathology is a great success in clinical diagnostics and surgical planning. However, MRI lacks sufficient specificity. This drawback is circumvented by recourse to MRS which has an excellent sensitivity, and such an advantage is inherited by MRSI as per design. Hence, MRSI preserves the two best features, sensitivity and specificity, of MRI and MRS, respectively. The advantage of MRSI over MRS is that the former exhibits full volumetric multivoxel coverage of the tissue, whereas the later is for a single voxel. This difference is clinically significant, since a single selected voxel might not be sufficiently representative of the whole tissue volume affected by the disease.

Despite the enumerated practical advantages over virtually all other competitive methods, both MRS and MRSI still necessitate a more thorough scrutiny beyond the initial investigations/success before their full clinical utility could be firmly established through evaluations and cross-verifications, especially against the corresponding histopathological findings, whenever these are available for correlations purposes.

7.2. *Key role of mathematics via signal processing, especially by the fast Padé transform*

It is remarkable that the full potential of MRS and MRSI in clinical practice is not made apparent by the direct availability of the final act of measurement, i.e. by the encoded time signal or FID. Encoded FIDs need to be interpreted by theory in order to extract the clinically useful information. This theory is a judicious combination of the spectral methods from mathematics, physics and chemistry applied to measured data. Specifically, it is through signal processing that the encoded FID and the ensuing theoretically generated spectrum are characterized by a set of parameters that capture the physico-chemical and bio-medical information from the examined tissue [1].

These parameters are physical quantities called spectral parameters, and they are given by a set of pairs of complex numbers that represent complex frequencies and complex amplitudes. Each such pair characterizes a given physical/genuine resonance/peak in the spectrum. The real and imaginary parts of the complex frequency are the chemical shift and the inverse of the relaxation time, T_2. The absolute value of the complex amplitude is proportional to the height of the resonant peak, with the constant of proportionality being the relaxation time of the same resonance. The phase of the complex amplitude is the phase of the FID. In this way, both the FID and the associated spectrum are simultaneously parameterized by quantitative mathematical methods of spectral analysis or signal processing.

Such a physico-mathematical parameterization of the results of encoding yields the sought bio-chemical and clinical characterization of the tissue content. Each metabolite, being a molecule, can exhibit one or more resonances in a studied spectrum. Therefore, once the results of spectral analysis become available, metabolite concentrations, as one of the most relevant clinical markers, can be deduced directly from the reconstructed spectral parameters. This quantitative analysis, accompanied with error analysis, must be carried out with utmost reliability for the obtained spectral parameters, regarding their total number, accuracy and stability against noise, in order that MRS and MRSI could maintain their proclaimed power of enhanced specificity. It is precisely here that *the mathematical theory of signal processing plays a decisive role*, and especially the fast Padé transform, FPT, is optimally suited for this demanding, challenging and vitally important task.

7.3. *Summary of open directions for urgent studies*

There is an urgent need for accurate quantification to determine metabolite concentrations, so that MRS can be better used to detect and characterize cancers, with clear distinction from non-malignant processes [7]. Metabolite concen-

trations can only be accurately computed if the spectral parameters are obtained in a reliable way with an intrinsic and robust error analysis. This is provided by the FPT.

We anticipate that MRS via Padé processing will reduce the false positive rates of MR-based modalities and further improve the sensitivity of these methods. Once this is achieved, and given that all MR-based diagnostic methods are free from ionizing radiation, new possibilities for cancer screening and early detection will open up, especially for risk groups, e.g. the application of Padé-optimized MRS in younger women at high risk for breast cancer. The need for accurate quantification of closely overlapping resonances has been particularly underscored for breast cancer diagnostics using MRS [18,19,31]. Moreover, MRS via Padé processing would be a promising avenue for early detection of ovarian cancer, which, is extremely problematic with the standard diagnostic methods. Further, MRS with the accompanying Padé quantification applied to prostate cancer is particularly important for diagnostic enhancement, because of the current dilemmas surrounding prostate cancer screening (e.g. cut-points of prostate specific antigen, etc), as well as the public health importance of this malignancy.

Overall, the methodologies reviewed in this study aim to enable Padé-based MRS to soon become a standard tool for clinical oncology [1,7]. This powerful and versatile signal processor is optimal for MRS, due to the usage of the unique rational polynomial approximation, which most naturally describes resonant peaks in molecular absorption spectra that stem from tissue.

As discussed, the Padé approximant is, in fact, the exact theory whenever the function to be modeled is itself given by a ratio of two polynomials. Such are the spectra from MRS. This hardly leaves any doubt as to which mathematical method is best suited for studying MRS. Such a conclusion extends automatically to MRSI which encounters precisely the same type of time signals as in MRS.

Time signals analyzed in this review are comprised of damped complex exponentials with either stationary or non-stationary amplitudes that correspond to non-degenerate (Lorentzian) or degenerate (non-Lorentzian) absorption spectra. This particular form is the correct mathematical and physical description of attenuated oscillatory motions of any system, since such modeling represents the most general expression for the auto-correlation functions or time signals predicted by the Schrödinger picture of quantum mechanics [1], which is universally applicable to all phenomena, including those occurring in living organisms.

Acknowledgments

This work was supported by King Gustav the Fifth's Jubilee Foundation, Karolinska Institutet (KI) Fonden and the Swedish Scientific Research Council (Vetenskapsrådet).

References

[1] Dž. Belkić, Quantum mechanical signal processing and spectral analysis (Institute of Physics Publishing, Bristol, 2004) [and references therein].

[2] Dž. Belkić, *Principles of Quantum Scattering Theory* (Institute of Physics Publishing, Bristol, 2003) [and references therein].

[3] Z.-P. Liang and P. Lauturber, *Principles of Magnetic Resonance Imaging: A Signal Processing Perspective* (IEEE Press Series in Biomedical Engineering, New York, 2000).

[4] F. Howe and K.S. Opstad, ^{1}H MR spectroscopy of brain tumours and masses, NMR Biomed. 16 (2003) 123.

[5] S. Nelson, Multivoxel magnetic resonance spectroscopy of brain tumors, Mol. Cancer Ther. 2 (2003) 497.

[6] K. Belkić and Dž. Belkić, Spectroscopic imaging through MR for brain tumour diagnostics, J. Comp. Meth. Sci. Eng. 4 (2004) 157.

[7] K. Belkić, *Molecular Imaging through Magnetic Resonance for Clinical Oncology* (Cambridge International Science Publishing, Cambridge, 2004) [and references therein].

[8] E. Danielsen and B. Ross, *Magnetic Resonance Spectroscopy Diagnosis of Neurological Diseases* (Marcel Dekker, Inc, New York, 1999).

[9] L. Brandão and R. Domingues, *MR Spectroscopy of the Brain* (Lippincott Williams & Wilkins, Philadelphia, Pennsylvania, 2004).

[10] J. Kurhanewicz, M.G. Swanson, S.J. Nelson and D.B. Vigneron, Combined magnetic resonance imaging and spectroscopic imaging approach to molecular imaging of prostate cancer, J. Magn. Reson. Imaging. 16 (2002) 451.

[11] R. Dhingsa, A. Qayyum, F.V. Coakley, Y. Lu, K.D. Jones and M.G. Swanson, Prostate cancer localization with endorectal MR imaging and MR spectroscopic imaging: effect of clinical data on reader accuracy, Radiology 230 (2004) 215.

[12] I. Thompson, D.K. Pauler, P.J. Goodman, C.M. Tangen, M.S. Lucia and H.L. Parmes, et al., Prevalence of prostate cancer among men with prostate-specific antigen level $\leqslant$ 4.0 ng per ml, N. Engl. J. Med. 350 (2004) 2239.

[13] R. Katz-Brull, P.T. Lavin and R.E. Lenkinski, Clinical utility of proton MR spectroscopy in characterizing breast lesions, J. Natl. Cancer Inst. 94 (2002) 1197.

[14] J. Griffiths A.R. Tate, F.A. Howe and M. Stubbs, as part of the Multi-Institutional Group on MRS Application to Cancer, Magnetic resonance spectroscopy of cancer—practicalities of multi-centre trials and early results in non-Hodgkin's lymphoma, Eur. J. Cancer 38 (2002) 2085.

[15] R.H. Dixon, NMR studies of phospholipid metabolism in hepatic lymphoma, NMR Biomed. 11 (1998) 370.

[16] S. Mukherji, S. Schiro, M. Castillo, L. Kwock, K.E. Muller and W. Blackstock, Proton MR spectroscopy of squamous cell carcinoma of the extracranial head and neck: in vitro and in vivo studies, Am. J. Neuroradiol. 18 (1997) 1057.

[17] J. Star-Lack, E. Adalsteinsson, M.F. Adam, D.J. Terris, H.A. Pinto and J.M. Brown, et al., In vivo ^{1}H MR spectroscopy of human head and neck lymph node metastasis and comparison with oxygen tension measurements, Am. J. Neuroradiol. 21 (2000) 183.

[18] K. Belkić, MR spectroscopic imaging in breast cancer detection: possibilities beyond the conventional theoretical framework for data analysis, Nucl. Instr. Meth. Phys. Res. A 525 (2004) 313.

[19] K. Belkić, Current dilemmas and future perspectives for breast cancer screening with a focus upon optimization of MR spectroscopic imaging by advances in signal processing, Isr. Med. Assoc. J. 6 (2004) 610.

[20] I. Gribbestad, B. Sitter, S. Lundgren, J. Krane and D. Axelson, Metabolite composition in breast tumors examined by proton nuclear MR spectroscopy, Anticancer Res. 19 (1999) 1737.

[21] M. Kaminogo, H. Ishimaru, M. Morikawa, M. Ochi, R. Ushijima and M. Tani, et al., Diagnostic potential of short echo time MR spectroscopy of gliomas with single-voxel and point-resolved spatially localised proton spectroscopy of brain, Neuroradiology 43 (2001) 353.
[22] I. Smith, and D.E. Blandford, Diagnosis of cancer in humans by 1H NMR of tissue biopsies, Biochem. Cell Biol. 76 (1998) 472.
[23] J. Wallace, G.P. Raaphorst, R.L. Somorjai, C.E. Ng and M.F.K. Fung, et al., Classification of 1H MR spectra of biopsies from untreated and recurrent ovarian cancer using linear discriminant analysis, Magn. Reson. Med. 38 (1997) 569.
[24] E. Boss, S.H. Moolenaar, L.F.A.G. Massuger, H. Boonstra, U.F.H. Engelke and J.G.N. de Jong, et al., High-resolution proton nuclear magnetic resonance spectroscopy of ovarian cyst fluid, NMR Biomed. 13 (2000) 297.
[25] L. Massuger, P.B.J. van Vierzen, U. Engelke, A. Heerschap and R. Wevers et al., 1H-MR spectroscopy. A new technique to discriminate benign from malignant ovarian tumors, Cancer 82 (1998) 1726.
[26] T.R. Brown, B.M. Kincaid and K. Uğurbil, NMR chemical shift imaging in three dimensions, Proc. Natl. Acad. Sci. USA, 79 (1982) 3523.
[27] Dž. Belkić and K. Belkić, The fast Padé transform in MR spectroscopy for improvements in early cancer diagnostics, Phys. Med. Biol. 50 (2005) 4385.
[28] P. Bottomley, The trouble with spectroscopy papers, J. Magn. Reson. Imaging 2 (1992) 1.
[29] K. Opstad, S.W. Provencher, B.A. Bell, J.R. Griffiths, and F.A. Howe, Detection of elevated glutathione in meningiomas by quantitative in vivo 1H MRS, Magn. Reson. Med. 49 (2003) 632.
[30] Y.-D. Cho, G-H. Choi, S-P. Lee and J-K. Kim, ^{1}H-MRS metabolic patterns for distinguishing meningiomas from other brain tumors, Magn. Reson. Imaging 21 (2003) 663.
[31] Dž. Belkić and K. Belkić, Mathematical optimization of in vivo NMR chemistry through the fast Padé transform: Potential relevance for early breast cancer detection by magnetic resonance spectroscopy, J. Math. Chem. 40 (2006) 85.
[32] Dž. Belkić, Fast Padé Transform for MRI and computerized tomography, Nucl. Instr. Meth. Phys. Res. A 471 (2001) 165.
[33] Dž. Belkić, Non-Fourier based reconstruction techniques, Magn. Reson. Mater. Phys. Biol. Med. 15 (2002) 36.
[34] Dž. Belkić, Exact analytical expressions for any Lorentzian spectrum in the fast Padé spectrum, J. Comp. Meth. Sci. Eng. 3 (2003) 109.
[35] Dž. Belkić, Strikingly stable convergence of the fast Padé transform, J. Comp. Meth. Sci. Eng. 3 (2003) 299.
[36] Dž. Belkić, Padé-based magnetic resonance spectroscopy (MRS), J. Comp. Meth. Sci. Eng. 3 (2003) 563.
[37] Dž. Belkić, Strikingly stable convergence of the fast Padé transform (FPT) for high-resolution parametric and non-parametric signal processing of Lorentzian and non-Lorentzian spectra, Nucl. Instr. Meth. Phys. Res. A 525 (2004) 366.
[38] Dž. Belkić, Analytical continuation by numerical means in spectral analysis using the fast Padé transform, Nucl. Instr. Meth. Phys. Res. A 525 (2004) 372.
[39] Dž. Belkić, Error analysis through residual frequency spectra in the fast Padé transform (FPT), Nucl. Instr. Meth. Phys. Res. A 525 (2004) 379.
[40] Dž. Belkić and K. Belkić, Fast Padé transform for optimal quantification of time signals from MR spectroscopy, Int. J. Quantum Chem. 105 (2005) 493.
[41] Dž. Belkić and K. Belkić, In vivo magnetic resonance spectroscopy by the fast Padé transform, Phys. Med. Biol. 51 (2006) 1049.
[42] Dž. Belkić, Exact quantification of time signals in Padé-based magnetic resonance spectroscopy, Phys. Med. Biol. 51 (2006) 2633.

[43] Dž. Belkić, Exponential convergence rate (the spectral convergence) of the fast Padé transform for exact quantification in magnetic resonance spectroscopy, Phys. Med. Biol. 51 (2006) 6483.
[44] Dž. Belkić, Fast Padé transform for exact quantification of time signals in magnetic resonance spectroscopy, Adv. Quantum Chem. 51 (2006) 157.
[45] W.W.F. Pijnappel, A. van den Boogaart, R. de Beer and D. van Ormondt, SVD-based quantification of magnetic resonance signals, J. Magn. Reson. 97 (1992) 122.
[46] J.W.C. van der Veen, R. de Beer, P.R. Luyten and D. van Ormondt, Accurate quantification of in vivo 31P NMR signals using the variable projection method and prior knowledge, Magn. Reson. Med. 6 (1988) 92.
[47] L. Vanhamme, A. van den Boogaart and S. van Haffel, Improved method for accurate and efficient quantification of MRS data with use of prior knowledge, J. Magn. Reson. 129 (1997) 35.
[48] S.W. Provencher, Estimation of metabolite concentrations from localized in vivo proton NMR spectra, Magn. Reson. Med. 30 (1993) 672.
[49] D. Williamson, H. Hawesa, N.A. Thacker and S.R. Williams, Robust quantification of short echo time 1H MR spectra using the Padé approximant, Magn. Reson. Med. 55 (2006) 762.
[50] Dž. Belkić, P.A. Dando, J. Main and H.S. Taylor, Three Novel High-Resolution Nonlinear Methods for Fast Signal Processing, J. Chem. Phys. 113 (2000) 6542.
[51] V. Govindaraju, K. Young and A.A. Maudsley, Proton NMR chemical shifts and coupling constants for brain metabolites, NMR Biomed. 13 (2000) 129.
[52] P. Swindle, S. McCredie, P. Russell, U. Himmelreich, M. Khadra, C. Lean and C. Mountford, Pathologic characterization of human prostate tissue with proton MR spectroscopy, Radiology 228 (2003) 144.
[53] R.J. McEliece and J.B. Shearer, A property of Euclid's algorithm and an application to Padé approximation, SIAM J. Appl. Math. 34 (1978) 611.
[54] R.D. Palmer and J.R. Cruz, An ARMA spectral analysis technique based on a fast Euclidean algorithm, IEEE Trans. Acoust. Speech. Sign. Process. 37 (1989) 1532.
[55] J. Frahm, H. Bruhn, M.L. Gyngell, K.D. Merboldt, W. Hanicke and R. Sauter, Localised high-resolution NMR spectroscopy using stimulated echos: initial application to human brain *in vivo*, Magn. Reson. Med. 9 (1989) 79.
[56] M. Callaghan, D.J. Larkman and J.V. Hajnal, Padé methods for reconstruction and feature extraction in magnetic resonance imaging, Magn. Reson.Med. 54 (2005) 1490.
[57] I. Tkáč, P. Andersen, G. Adriany, H. Merkle, K. Uğurbil, and R. Gruetter, In vivo 1H NMR spectroscopy of the human brain at 7 T, Magn. Reson. Med. 46 (2001) 451.
[58] C.E. Mountford, C.L. Lean and R. Hancock, Magnetic resonance spectroscopy detects cancer in draining lymph nodes, Invas. Metast. 13 (1993) 57.
[59] C.E. Mountford, S. Doran, C. Lean and P. Russell, Proton MRS can determine the pathology of human cancers with a high level of accuracy, Chem. Rev., 104 (2004) 3677.
[60] P. Malycha, Sentinel lymph node biopsy, ANZ J. Surg. 73 (2003) 370.
[61] L. Gluch, Magnetic resonance in surgical oncology: I On the origin of the spectrum, ANZ J. Surg. 75 (2005) 459.
[62] L. Gluch, Magnetic resonance in surgical oncology: II Literature review, ANZ J. Surg. 75 (2005) 464.
[63] F. Jolesz, Future of magnetic resonance imaging and magnetic resonance spectroscopy in oncology, ANZ J. Surg. 75 (2005) 372.